# A METALLIC-GLASS RIBBON REINFORCED GLASS-CERAMIC MATRIX COMPOSITE

By

Rajendra Uddhav Vaidya

A THESIS

Submitted to
Michigan State University
in partial fulfillment of the requirements
for the degree of

DOCTOR OF PHILOSOPHY

Department of Metallurgy, Mechanics and Materials Science

1991

## ABSTRACT

### A METALLIC-GLASS RIBBON REINFORCED GLASS-CERAMIC MATRIX COMPOSITE

By

Rajendra Uddhav Vaidya

The feasibility of producing metallic-glass ribbon reinforced glass-ceramic composites by low cost pressing and sintering techniques was demonstrated. The quality of the composite specimens produced was affected by factors such as binder content, compaction pressure and sintering temperature. The mechanical behavior of such composites was studied and the failure modes could be correlated to variations in the matrix strength and interfacial bond strength with temperature.

The fracture toughness of such composites was dependant on the ribbon orientation (with respect to its long and short transverse faces) and ribbon layout in the matrix. This was primarily attributed to differences in the moments of inertia of the ribbons in

the different orientations. The load transfer characteristics of this composite system was found to be different from those of other fiber reinforced systems. The ribbon width was found to play a significant role in the stress transfer between the component phases.

Discontinuous metallic-glass reinforced glass-ceramic matrix composites were also fabricated. The mechanical strength of such composites was found to be within 80% of the strength of a continuously reinforced composite containing the same volume fraction of reinforcements. The strength of such composites was also found to be isotropic in the plane of compaction.

## ACKNOWLEDGEMENTS

First and foremost I would like to thank my adviser Professor K. N. Subramanian for all his encouragement, help and support, without which this work would not have been possible. I would also like to thank my comittee members Professor E. D. Case and Professor N. J. Altiero of the Department of Metallurgy, Mechanics and Materials Science and Professor H. Eick of the Department of Chemistry for their valuable suggestions from time to time. I would also like to express my gratitude to Dr. L. T. Drzal and the Composite Materials and Structures Center at Michigan State University for supporting and funding this project. Thanks are also due to Professor K. Mukherjee and all other faculty, staff and students of the Department of Metallurgy, Mechanics and Materials Science for their support. Last but not least, I would like to thank my parents and sister for their support.

## TABLE OF CONTENTS

**ABSTRACT:**

Metallic-glass ribbon reinforced glass-ceramic matrix composites were fabricated by conventional wet pressing and sintering techniques. Some of the important aspects of composite fabrication have been discussed here. Variables such as binder content, compaction pressure and specimen size, and their interdependancy on one another are discussed. The optimum processing conditions required to obtain the best specimens will be stated. The sintering temperature was also found to be very important. The sintering temperature not only controls the softening characteristics of the parent glass, but also affects the specimen distortion. Proper selection of the sintering temperature can ensure minimum distortion in the specimens, while at the same time retain the ease and efficiency of fabrication.

## INTRODUCTION:

Developments in fiber reinforced ceramic matrix composites have proceeded at a rapid pace in the past few years [1]. Various types of fibers, especially silicon carbide, alumina and carbon, have become very popular as reinforcements for these brittle ceramic matrices because of the high strength and toughness they impart when incorporated into the ceramic matrices.

The three classes of ceramic matrices commonly employed are glasses, glass-ceramics and crystalline ceramics. Glass matrices, although easy to fabricate because of the softening they exhibit, are also handicapped by low useful operating temperatures for the very same reasons. Crystalline ceramic matrices are relatively difficult to process, but have relatively higher use temperatures. These matrices are usually fabricated by powder pressing techniques which invariably result in some amount of retainedporosity in the structure. This porosity although small in magnitude, can result in a severe deterioration of the mechanical properties of the system. Techniques such as hot-isostatic pressing, vapor deposition and sol-gel

method have been employed to either obtain a finer particle size or densify the structure, but have only been achieved at the expense of increased costs and/or low productivity rates (because of the relatively long processing times).

Glass-ceramics combine the advantages of both the glassy and crystalline materials. The glass-ceramics are fabricated in the glassy state, and hence relatively lower temperatures can be used as compared to those required in the fabrication of the crystalline ceramics. Upon fabrication, the glassy matrix is converted to a crystalline state. This crystalline state does not exhibit softening, and hence the resultant glass-ceramic can be used at temperatures close to the melting point of the crystalline phase, which is usually much higher than the softening point of the parent glass. Proper selection of the parent glass can result in a glass-ceramic during the fabrication step itself, saving time and cost for a seperate heat treatment step. These glass-ceramics also have a significantly lower amount of porosity as compared to crystalline ceramics processed under similar conditions. Various glass-ceramics being actively investigated recently include LAS (Lithium alumino silicates) and MAS (Magnesium alumino silicate)

systems.

Metallic-glasses are an interesting class of materials being studied. Metallic-glasses are produced by rapid solidification of molten metal. High rates of cooling are employed for the same (of the order of $10^6$ to $10^9$ $^oK/sec$), and crystallization of the molten metal is suppressed. The resultant structure of the material has no long range order and is referred to as being `amorphous'.

Metallic-glasses possess unique mechanical properties. They are extremely strong and hard, and are very tough. They are also more oxidation and corrosion resistant as compared to the parent metal from which they are derived. The ribbon geometry is a natural consequence of the high cooling rates required in the manufacture of these metallic-glasses. This ribbon geometry provides for an extremely large surface area. Another interesting feature of these metallic-glasses is their ability to be bent to almost a zero radius with very little plastic deformation. This ability of the metallic-glasses makes them extremely damage tolerant.

Metallic glasses have been investigated as

reinforcements for polymer [2-5] and metal [6] matrices. These studies indicated that significant improvements in the mechanical properties could be achieved with relatively small volume fractions of reinforcements. The potential of using metallic-glasses as reinforcements for brittle glass-ceramics was not demonstrated until recently [7-12]. These studies also indicated the tremendous potential of developing such composites for structural applications. In addition to the improved properties, it should also be noted that relatively easy and cost efficient techniques were used in the fabrication of the same. Both continuously and discontinuously reinforced composites were fabricated.

In this paper, some of the aspects of fabrication of such metallic-glass ribbon reinforced glass-ceramic matrix composites will be presented. The various fabrication parameters and their effect on the fabrication processes will be discussed. Some of the practical problems encountered in the fabrication of such composites will also be emphasized. The important point to keep in mind here is that all of these experiments resulted in the fabrication of laboratory sized small specimens. No commercial component was fabricated. Hence problems related to scaling up will have to be considered seperately if such composites

have to be fabricated for commercial applications.

## EXPERIMENTAL METHODS:

### Starting Materials:

Two commercially available metallic-glasses namely METGLAS MBF-75 and METGLAS MT 2605S-2 were selected as the reinforcements. This selection was based on two important factors; good mechanical properties and relatively higher crystallization temperatures. METGLAS is a trademark of Metglas Corp., a subsidiary of Allied Signal Ltd for brazing metals and alloys, and both the metallic-glasses used were obtained from them. Since the production of METGLAS MBF-75 has been discontinued, most of the latter studies were carried out on composites incorporating METGLAS 2605S-2. The physical and chemical properties of these metallic-glasses as provided by the manufacturer are given in Table 1.

The crystallization temperature of the metallic-glasses dictated the choice of the selected glass matrices. Both the metallic-glasses had crystallization temperatures in the range of 550$^{o}$C.

TABLE 1: Physical properties and chemical compositions of the metallic-glass ribbon reinforcements.

| Property | Metglas 2605S-2 | Metglas MBF-75 |
|---|---|---|
| Chemical composition (%) | Fe 78<br>B 13<br>Si 9 | Ni 50<br>Co 23<br>Cr 10<br>Mo 7<br>Fe 5<br>B 5 |
| Crystallization temperature($^{o}$C) | 550 | 605 |
| Elastic modulus (GPa) | 85 | 70 |
| Yield strength (MPa) | >700 | 1300 |
| Coefficient of ($^{o}C^{-1}$) | $76 \times 10^{-7}$ | $78 \times 10^{-7}$ |
| Density (g $cm^{-1}$) | 7.18 | 7.46 |

Hence it was critical to select glass matrices having softening temperatures below 550°C. Heating up a metallic-glass above its crystallization temperature usually results in a loss of mechanical properties. In fact it has been shown that the mechanical properties of this metallic-glass begin to degrade far below its crysatllization temperature (Table 2). However the loss of strength was not that significant, and a large portion of the initial strength and toughness of the metallic-glass can be retained if the temperature is maintained 100-150°C below the crystallization temperature of the metallic-glass.

Based on all of these requirements, Corning Glass Codes 7572 and 8463 were initially selected as potential matrices. However, based on mechanical property considerations, the 7572 matrix was found to be superior as compared to the 8463 matrix. Subsequent tests were conducted on specimens fabricated using the 7572 matrix only. Some of the properties of the matrices as provided by the manufacturer are given in Table 3.

**Equipment used:**

The metallic-glass reinforced glass-ceramic

TABLE 2: Measured tensile strength (in MPa) of the METGLAS 2605S-2 ribbon as a function of temperature and time.

| temp(°C) | time(min) 20 | 30 | 60 | 120 | 180 | 300 |
|---|---|---|---|---|---|---|
| 100 | -- | 2059 | 1464 | 2236 | --- | 1426 |
| 200 | -- | 1987 | 1842 | 2114 | --- | 1420 |
| 300 | -- | 1894 | 1733 | 2328 | --- | 1905 |
| 400 | -- | 1028 | 1102 | 986 | 972 | --- |
| 450 | 1709 | -- | 775 | 851 | 724 | --- |
| 550 | -- | 443 | -- | --- | --- | --- |

TABLE 3: Physical properties and chemical compositions of the glass matrices as provided by the manufacturer.

| Property | Corning Glass 7572 | Corning Glass 8463 |
|---|---|---|
| Softening point ($^{o}C$) | 375 | 370 |
| Coefficient of thermal expansion ($^{o}C^{-1}$) | $95 \times 10^{-7}$ | $105 \times 10^{-7}C$ |
| Density (powder) gm/cc (fired) | 3.8<br>6.0 | 3.8<br>6.2 |
| Continuous service temperature ($^{o}C$) | 450 | 450 |
| Chemical composition (%) | PbO 70<br>$B_2O_3$ 5-10<br>$SiO_2$ 2-5<br>$Al_2O_3$ 1-5<br>ZnO 10-20 | PbO 84<br>$B_2O_3$ 5-10<br>$SiO_2$ 2-5<br>$Al_2O_3$ 1-5<br>ZnO 10-20 |

matrix composites were fabricated in steel dies. Two different geometries (cylindrical and prismatic) were employed for the purpose. In the prismatic geometry two different sizes were used.The steel dies were fabricated out of medium carbon alloy steel (4340), and heat treated to a hardness of 50 $R_C$. The dies with the rectangular cavities had a 'split' arrangement in order to facilitate specimen removal (Figure 1 a and b).

A Tinius-Olsen machine was used for compacting the powders in the dies. The machine had a maximum rated capacity of 60,000 lbs. Figure 2 shows the experimental setup used.

**Specimen fabrication:**

**a). Continuously reinforced composites:**

The metallic-glasses were obtained in the form of long continuous ribbons, about 2 inches wide (Figure 3). The ribbon was wound on a spool. The average thickness of the ribbons as measured was 25 microns. The ribbons were cut using an extremely sharp pair of scissors. One interesting point to note was that cutting the ribbons in a direction perpendicular to its

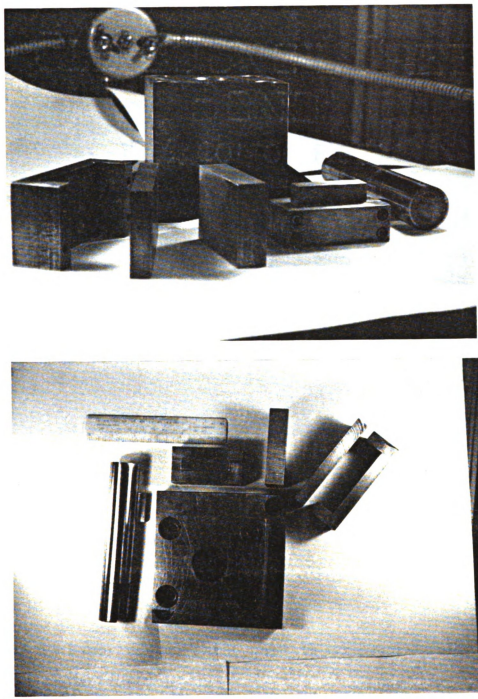

FIGURE 1: Dies used in the fabrication of the composite specimens.

a. Different sizes and geometries used

b. Split die assembly

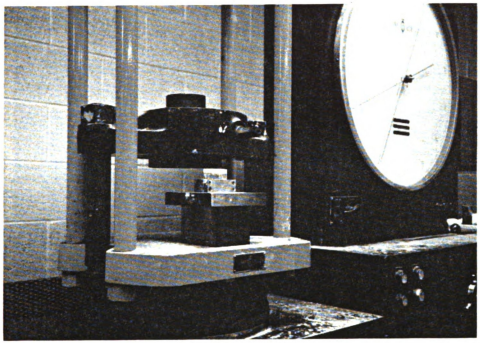

FIGURE 2: Experimental setup used in composite specimen fabrication.

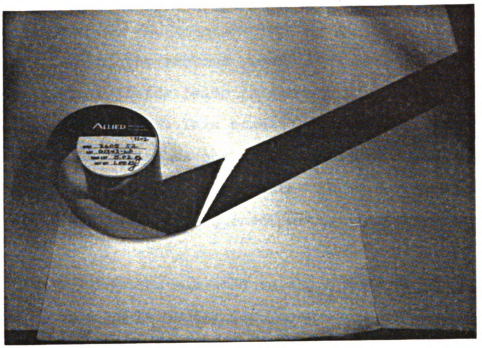

FIGURE 3: The metallic-glass ribbon reinforcement spools as obtained from the manufacturer.

width resulted in a relatively jagged and irregular cut. On the other hand, cutting the ribbons along the width was relatively easy, and did not lead to an irregular edge.

Cutting the ribbons caused them to bend slightly towards their inside (side in contact with the rollers during fabrication). This bending was an important factor which had to be accounted for during specimen fabrication. All the ribbons were thoroughly cleaned with acetone before being incorporated into the matrix.

Amyl acetate was used as the binder for the glass powder. This binder was recommended by the manufacturer (Corning Inc.). However the amount of binder used varied from the amount suggested by the manufacturer (3% by weight). Various factors influencing the amount of binder used included the size of the specimen and volume fraction of ribbons being incorporated into the specimens.

Care was taken to ensure complete binder removal before sintering the specimen. The specimens were preheated to 250$^{o}$C for sufficient periods of time before being sintered. In cases where larger amounts of binder were used, even longer times were employed.

Binder removal was determined relatively easily because of the extremely strong odor which was emitted during vaporization of the binder.

In order to fabricate the continuously reinforced composites, the glass powder was weighed out, and mixed with appropriate amounts of amyl acetate binder. A small amount of powder was placed in the die and pre-pressed. The sized metallic-glass ribbons were then laid down within the die over this pre-pressed lower layer. Care was taken to see that the concave surface of the ribbon (bent) always faced upwards. Avoiding this led to the formation of cracks in the green compacts. After the required volume fraction of ribbons were incorporated into the matrix, a final layer of matrix material was placed at the top and the whole compact was pressed.

The compaction pressure was applied very slowly in order to ensure uniform density distribution within the compact. The amount of pressure used depended on two important factors; the thickness of the specimen and the binder content.

After compaction, the specimens were removed from the die. The `split' assembly of the dies made

specimen withdrawl extremely easy. However, sometimes the specimens did stick to the die cavity. Use of a light machine oil to lubricate the die cavity was found to remedy the situation, although a small amount of oil did get absorbed within the specimen.

The green compacts were then laid out on stainless steel or alumina plates. In order to prevent the specimens from sticking to the plates, they were either coated with a thin film of graphite or covered with an extremely thin foil of aluminum, which was easily peeled off after fabrication (Figure 4).

As mentioned earlier, sintering of the specimen was preceeded by a binder burnoff stage. Sintering was carried out in an air atmosphere at 400$^{o}$C. The sintering time varied depending on the specimen, and usually ranged between 1-5 hours. The sintering stage was accompanied by a heat treatment at 450$^{o}$C, which converted the glassy matrix into a crystalline state. Time for the crystallization treatment varied between 20 minutes and 1 hour. The main crystalline phase was 2PbO.ZnO. After crystallization, the specimens were furnace cooled down to room temperature.

All the specimens experienced an adequate amount

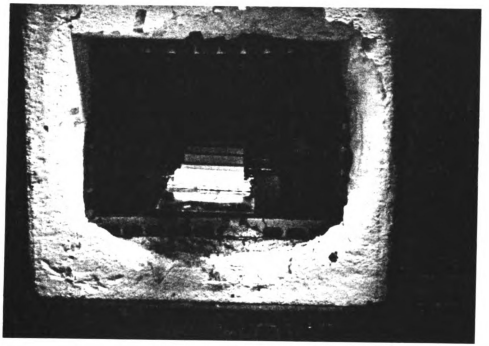

FIGURE 4: Loading the green compacts in the furnace for sintering.

of flow during the sintering stage. Due to this all the specimens had rounded upper edges. Some amount of polishing was required to restore the required shape. However, the dimensions of the polished specimens were always within 30% of the dimensions of the corresponding green compacts.

b).Discontinuously reinforced composites:

The procedure used in the fabrication of these composites was more or less similar to the one described earlier. The metallic-glass ribbons were sized to appropriate dimensions. After sizing, the ribbons were precoated with the glass powder. Precoating was done by preparing a slurry of the glass powder with excess of amyl acetate binder, and incorporating the ribbons within the slurry. The slurry was then heated up to 250$^{o}$C to remove the binder. This was then mixed with more glass powder containing a relatively smaller amount of binder. After mixing, compaction in the die was carried out, followed by sintering and crystallization. In spite of the higher pressure used, the green compact strength of the specimen was very poor and more than 60% of the specimen had to be discarded because of cracking problems.

**DISCUSSION:**

The variation in the compaction pressure with binder content is shown in Figure 5. From the figure it can be seen that the compaction pressure decreases with increasing binder content. However for pressures exceeding 5000 psi, pressure cracking was observed in the specimens, irrespective of the binder content used. Compaction pressures less than 200 psi were also found to be insufficient to impart enough green strength to the compacts. Binder contents in excess of those determined by the curve led to the excess binder being squeezed out of the sides of the die. The combination of binder content and compaction pressure used are indicated in the figure.

The variation in the time required for binder removal with preheat temperature is shown in Figure 6. Shorter preheating times were required at higher temperatures. However, the preheat temperature had to be maintained below the softening temperature of the glass matrix in order to prevent any pores from getting trapped in the matrix during the glass flow. A temperature of 250$^{o}$C was found to be most suitable. Higher temperatures led to shorter preheating times, but also caused cracks to form in the compacts,

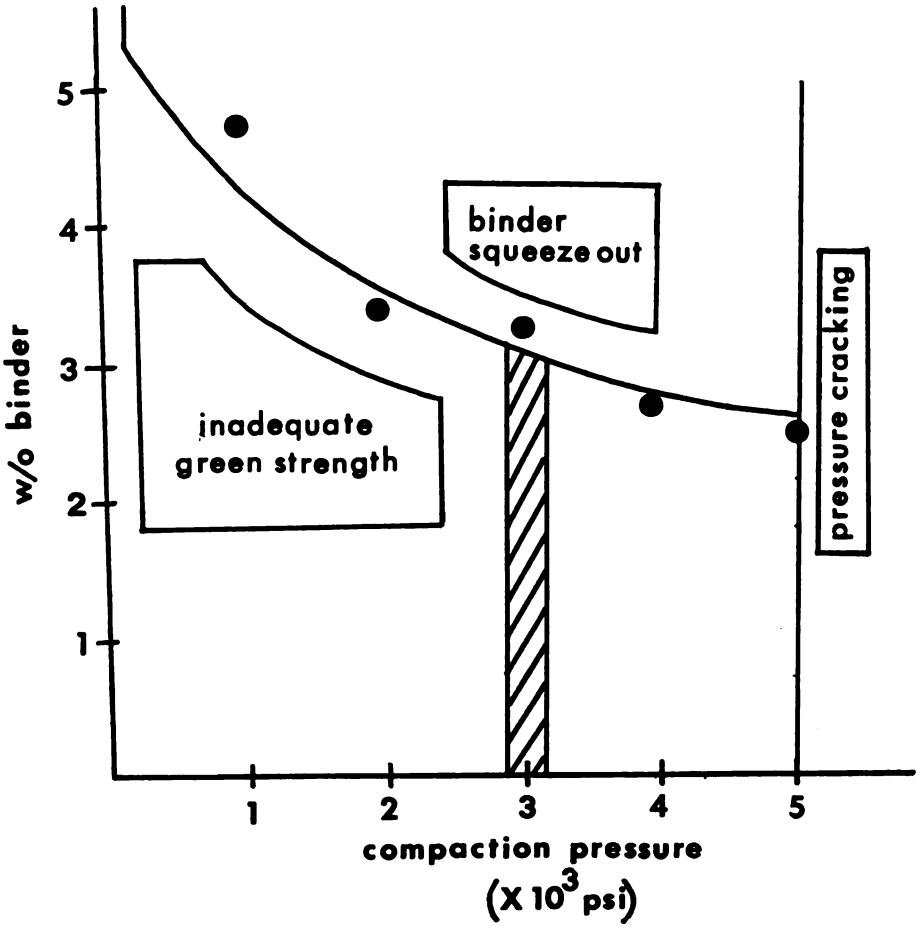


FIGURE 5: Variation in the compaction pressure with binder content.

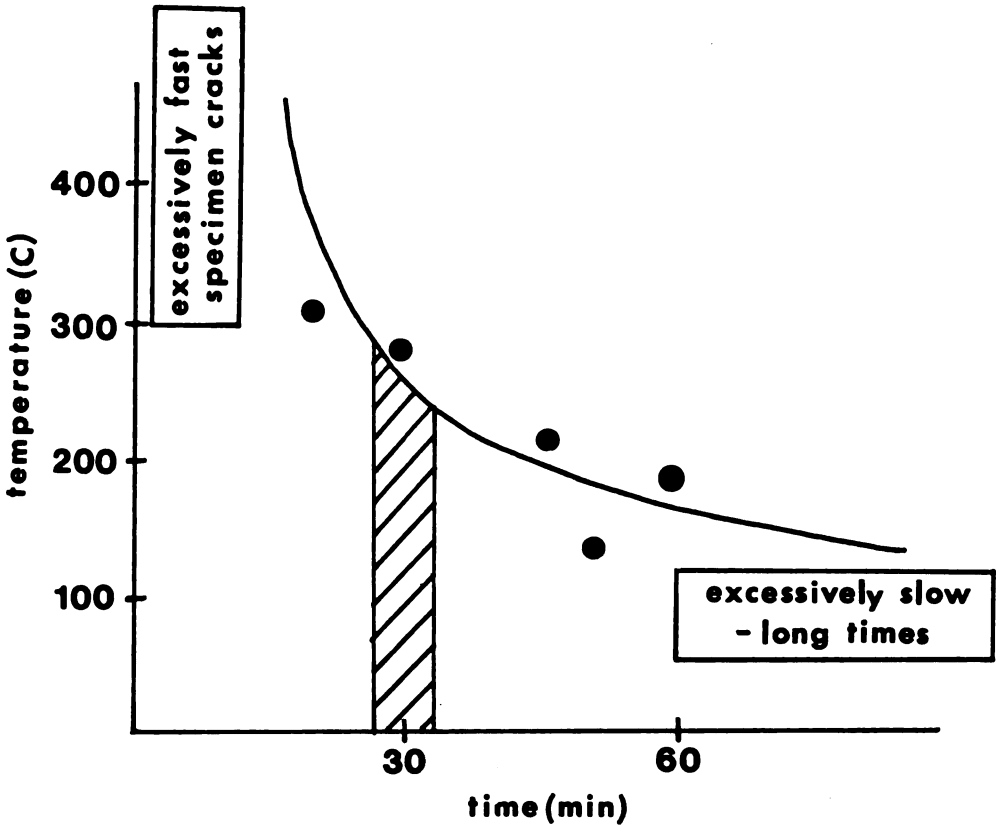


FIGURE 6: Variation in the time required for binder removal as a function of the preheat temperature.

probably as a result of the binder vaporizing too quickly.

Heating the compacts to the softening point and above led to glass flow, which in turn caused the specimens to change in dimensions. Flow of the glass matrix usually caused the specimen thickness to decrease, and specimen width to increase. This flow in the specimens was measured by calculating the change in the specimen thickness as compared to the thickness of the original green compacts. The specimen dilation as a function of increasing time, for different temperatures is shown in Figure 7. For temperatures below the crystallization temperature of the glass matrix, increasing times led to increased glass flow. At the crystallization temperature, the specimen dilation increased initially, but then decreased as the crystallization process progressed. Crystallization of the matrix led to an increase in the viscosity of the matrix.

The equation one can use to predict the dilation due to matrix flow (between 370$^{o}$C and 450$^{o}$C) has the form

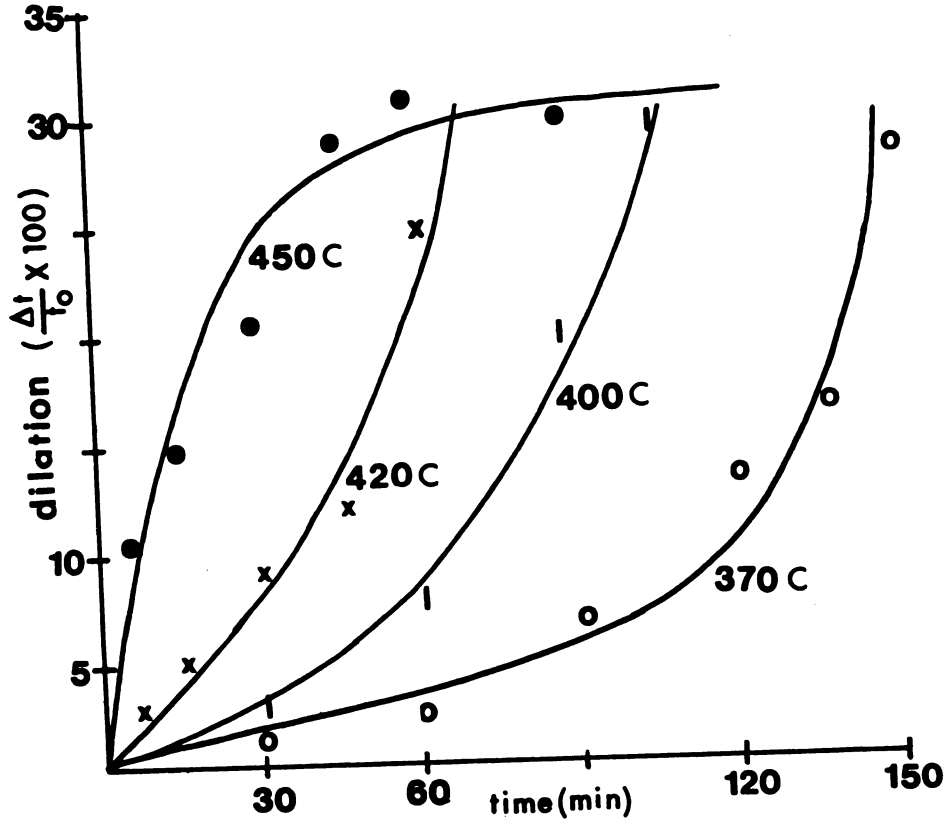


FIGURE 7: Specimen distortion as a function of time for different temperatures.

$$R = C \exp [Bt - D/t] \quad \ldots\ldots\ldots\ldots (1)$$

where, R is the specimen dilation defined as (change in specimen height)/(original height)

t is the time, and

B, C, and D are constants based on curve fitting

For t = 0, the dilation is zero, and

for t = infinity , the dilation is infinite.

For very large times, the equation can be approximated to

$$R = C \exp [Bt] \quad \ldots\ldots\ldots\ldots\ldots\ldots (2)$$

For a given temperature and large times, B and C can be taken as constants. In order to determine these constants differenciate both sides of equation 2.

Hence,

$$\frac{d(R)}{d(t)} = B\ C \exp (Bt)$$

$$= B\ R$$

Hence,

$$\frac{d(R)}{d(t)} - B\,R = 0 \qquad \ldots\ldots\ldots\ldots\ldots\ldots (3)$$

This equation can be used to determine the constants B and C for different temperatures. Choosing points in the regions corresponding to longer time periods in each curve in Figure 7, the values of B and C can be obtained as

| Temperature | B ($sec^{-1}$) | C |
|---|---|---|
| 370°C | $7.14 \times 10^{-3}$ | 16.52 |
| 400°C | 0.01 | 9.197 |
| 420°C | 0.017 | 2.314 |

To obtain the value of D, one can use Equation 1 and choose points in the regions corresponding to shorter times of the curve (assuming B and C remain constant). The values of D obtained are

| Temperature | D (sec) |
|---|---|
| 370°C | 87.30 |
| 400°C | 36.15 |
| 420°C | 0.81 |

For temperatures below the crystallization temperature, one can assume that the viscosity of the matrix is independant of time. However at 450°C, the viscosity becomes a function of time and temperature. This is because as time progresses, more and more of the matrix crystallizes and causes the viscocity to increase. The equation for the dilation takes the form

$$R = C(T,t) \exp [B(T,t)t] \quad \ldots\ldots\ldots\ldots (4)$$

As the temperature increases the pre exponent term C decreases and its effect on the dilation becomes less important as compared to the exponent term. Hence we can assume that C is a constant (k) for practical

purposes. Equation 4 then takes a form

$$R = k \exp [B(T,t)t] \quad \ldots\ldots\ldots\ldots\ldots\ldots (5)$$

Determining B here is difficult because it is a function of time and temperature. In the limiting case for two times $t_1$ and $t_2$ very close to one another

$$\frac{R_1}{R_2} = \frac{\exp [Bt_1]}{\exp [Bt_2]} \quad \ldots\ldots\ldots\ldots\ldots\ldots\ldots\ldots (6)$$

Equation 6 can be used to find out the value of B as a function of temperature. This can be carried out by choosing points in various portions of the curve very close to one another. Variation in the constant B with increasing time is shown in Figure 8. From the figure it can be seen that B decreases as a function of time as a result of the crystallization process.

These results are useful for determining the

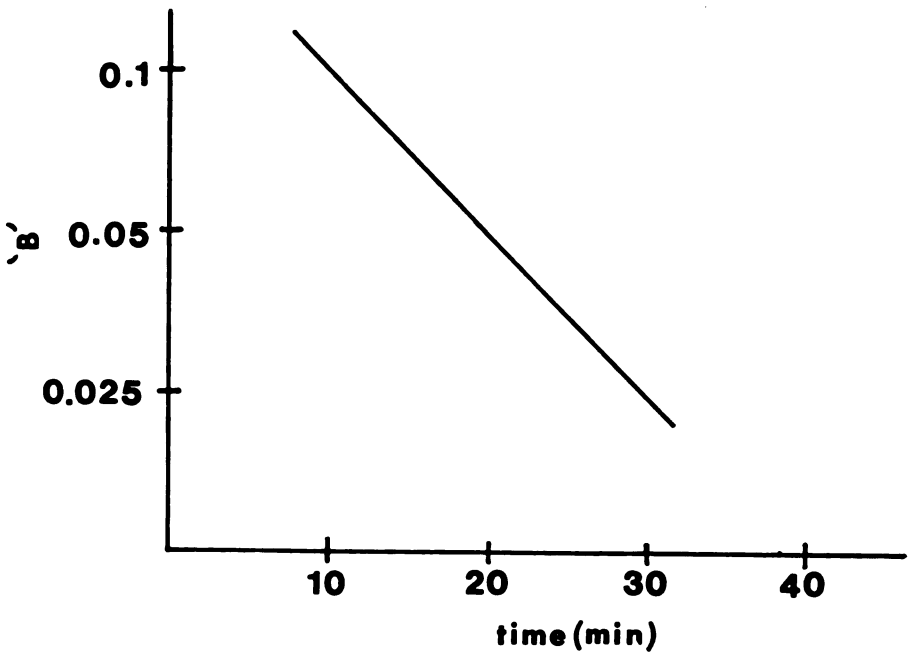


FIGURE 8: Variation in B as a function of time at 450°C.

optimum sintering temperature and time. For sintering it is necessary to have adequate flow but not too much so as to cause extensive distortion in the specimens. Sintering at the softening temperature of 370$^{o}$C was found to take too long. On the other hand sintering at 450$^{o}$C was completed in a short period of time but was accompanied by a large amount of distortion. Crystallization of the glass matrix occuring at this temperature was also found to be detrimental to the fabrication process (because crystallization was accompanied by an increase in the viscosity). Specimens fabricated at these temperatures were found to exhibit features similar to "cold shuts" (Figure 9). Fabricating at 400-420$^{o}$C was found to give the best specimens (Figure 10).

Some of the features observed on the fracture surfaces can be seen in the accompaning scanning electron micrographs (Figures 11 a, b, c and d). Important features to note in these micrographs are the strong bonding between the matrix and the ribbon reinforcements, and negligible porosity in the matrix.

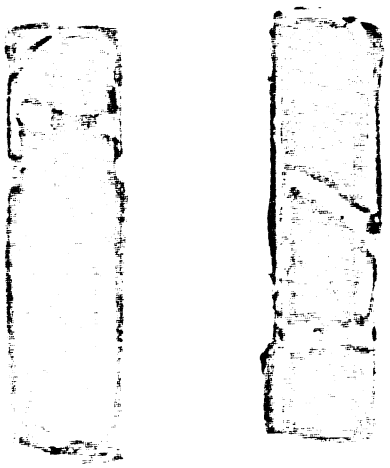

450

FIGURE 9: Inadequate glass flow in specimens sintered at 450°C.

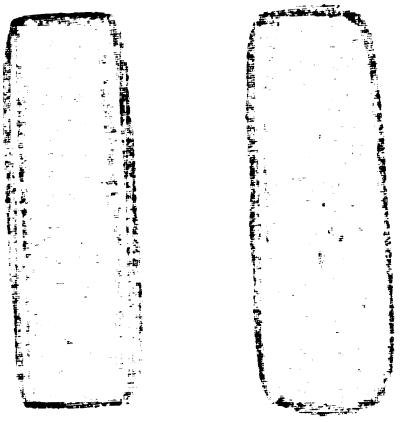

400

FIGURE 10: Specimens sintered at 400$^{o}$C.

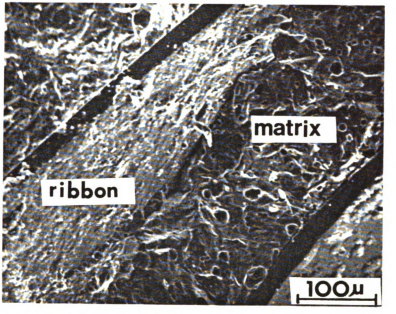
matrix
ribbon
100μ

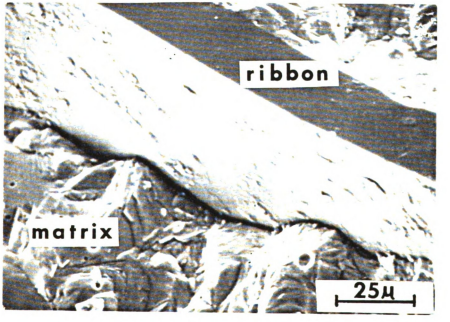
ribbon
matrix
25μ

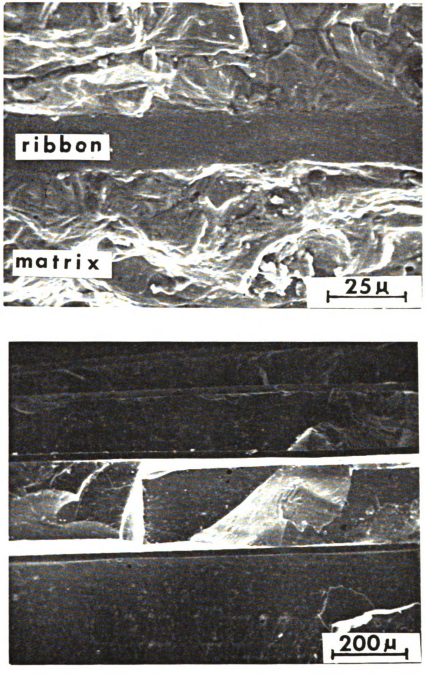


FIGURE 11: Fractured surfaces of the composite specimens.

a. Presence of good ribbon-matrix bonding.

b. Matrix material adhering to the ribbon surface.

c. Good ribbon-matrix bonding and negligible porosity in the matrix.

d. Multiple ribbon composite.

## SUMMARY:

This paper dealt with some of the aspects of the fabrication of metallic-glass ribbon reinforced glass-ceramic matrix composites. It has been shown that such composites can be produced by relatively low cost wet pressing and sintering techniques. Variables such as sintering temperature, binder content and sintering time are important and need to be carefully controlled to obtain good specimens.

## ACKNOWLEDGEMENTS:

The authors would like to acknowledge the support of the Composites Materials and Structures Center at Michigan State University. The authors would also like to thank Mr. Micheal Brykalski for the data provided in Table 2.

**REFERENCES:**


1. Tai-il Mah, Mendiratta M., Katz A. and Mazdiyasni S., Ceramic Bulletin, Vol.66, No.2, (1987) p. 304.
2. Strife J. and Prewo K., AFWAL Report TR-80-4060, 1980.
3. Strife J. and Prewo K., Journal of Materials Science, Vol.17, (1982) p. 359.
4. Fels A., Friedrich K. and Hornbogen E., Journal of Materials Science Letters, Vol.3, (1984) p. 569.
5. Friedrich K., Fels A. and Hornbogen E., Composites Science and Technology, Vol.23, (1985) p. 79.
6. Cytron S., Journal of Materials Science Letters, Vol.1, (1982) p. 211.
7. Vaidya R. U. and Subramanian K. N., Journal of Materials Science, Vol.25, (1990) p. 3291.
8. Vaidya R. U. and Subramanian K. N., ASM/ACCE/ESD Conference Proceedings, Detroit, Oct.89 published by ASM, Metals Park, Ohio, p. 227.
9. Vaidya R. U. and Subramanian K. N., Journal of Materials Science (in press).
10. Vaidya R. U. and Subramanian K. N., Journal of American Ceramic Society (in press).
11. Vaidya R. U., Lee T. K. and Subramanian K. N., ASC Conference Proceedings, E-Lansing, June 90, published by

Technomic press, Lancaster PA, p. 902.

12. Vaidya R. U. and Subramanian K. N., Composites Science and Technology (in press).

# CHAPTER 2

**ABSTRACT:**

Effect of temperature on the modulus of rupture of glass-ceramic matrix composites reinforced with very small volume fractions (~1%) of continuous metallic-glass ribbons was studied. The failure modes in such composites were found to significantly depend on the test temperature. Variations in the strength of the matrix, and the interfacial shear strength between the matrix and the ribbons due to changes in the test temperature, were found to control the elevated temperature strength and failure mode of these composites.

## INTRODUCTION:

Reinforcement of brittle matrices with high strength fibers results in dramatically improved mechanical properties such as increased toughness and high strain to failure. Recent developements [1-6] have led to a renewed interest in continuous fiber reinforced ceramic matrix composites for high temperature applications. Metallic-glass reinforcements in the form of ribbons possessing large surface areas and large aspect ratios have been demonstrated to be very effective in enhancing the mechanical properties of glass-ceramic matrices [7,8]. Even very small volume fraction of metallic-glass reinforcements were found to improve the strength, elastic properties and fracture toughness of the glass-ceramic matrices quite significantly. One of the potential use of such composites is at elevated temperatures, since glass-ceramics do not exhibit softening, unlike the parent glass from which they are derived. Successfull application of such metallic-glass ribbon reinforced glass-ceramic composites for high temperature applications depends on the characterization of their mechanical response at elevated temperatures. An understanding of the failure

mode at elevated temperatures is also important to make "life-time" predictions.

**EXPERIMENTAL PROCEDURE:**

Rectangular bar shaped composite specimens (5 cm x 1.5 cm x 0.4 cm) were prepared by using Corning Glass Code 7572 as the matrix and METGLAS MT 2605S-2 continuous ribbons as the reinforcements. The specimens were prepared by cold pressing and sintering techniques. Details of the chemical compositions of the ribbon and matrix, and composite manufacturing techniques have been described elsewhere [7].

Three point bending tests were carried out in an Instron testing machine with a cross head speed of 0.05 cm/min, in accordance to A.S.T.M standard C-203/85. Elevated temperature tests were carried out by heating the specimen and the test fixture, with an electrical resistance furnace. The temperature of the furnace was controlled to within + $5^{o}$ C. The specimens were soaked at the test temperature for 30 minutes prior to the tests. All the bending tests were performed in a nitrogen atmosphere to prevent oxidation of the fixture. A total of three specimens were tested at each temperature. Pullout tests were also carried out at various temperatures to measure the ribbon-matrix interfacial bond strength.

## RESULTS AND DISCUSSION:

Plots of the Modulus of Rupture (MOR) of the unreinforced matrix and composite specimens as a function of test temperature are provided in Figure 1. All the specimens were observed to retain most of their room temperature strength even at about 400°C. The composite specimens exhibited higher MOR values as compared to the unreinforced glass-ceramic matrix specimens at all temperatures tested. At higher temperatures matrix creep became predominant.

The load-deflection curves of the unreinforced matrix and composite specimens (containing 1.25 volume percent of reinforcements) at various temperatures are provided in Figures 2 and 3 respectively. At lower temperatures (upto 200°C) the composite exhibited typical brittle behaviour, with no evidence of ribbon-matrix debonding and sliding. At 300°C, a dramatic change was observed in the load-displacement curve, with the composite exhibiting ribbon debonding and sliding, accompanied by a large elongation to failure. At 400°C, although the matrix began to creep, the composite still retained a large portion of its strength. At 500°C, extensive matrix creep occured and

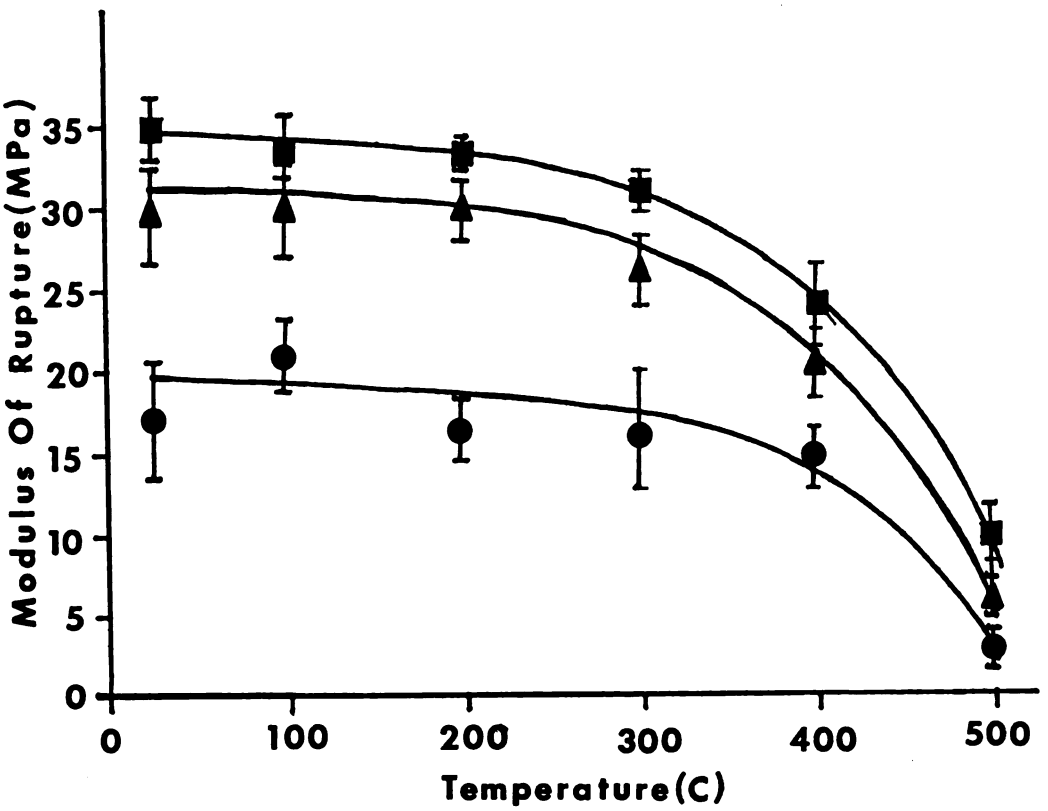


FIGURE 1: Plot of the Modulus of Rupture of the matrix and composite specimens as a function of temperature.

( ● Matrix, ▲ Composite with 0.73% by volume of ribbons and ■ Composite with 1.25% by volume of ribbons.)

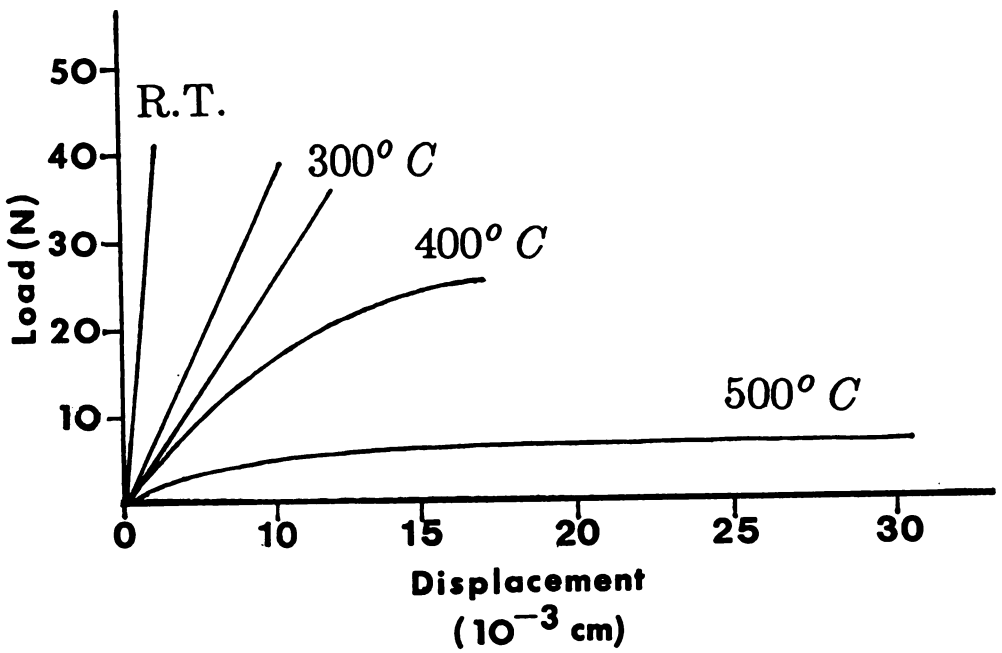


FIGURE 2: The load-displacement curves of the matrix specimens at various temperatures.

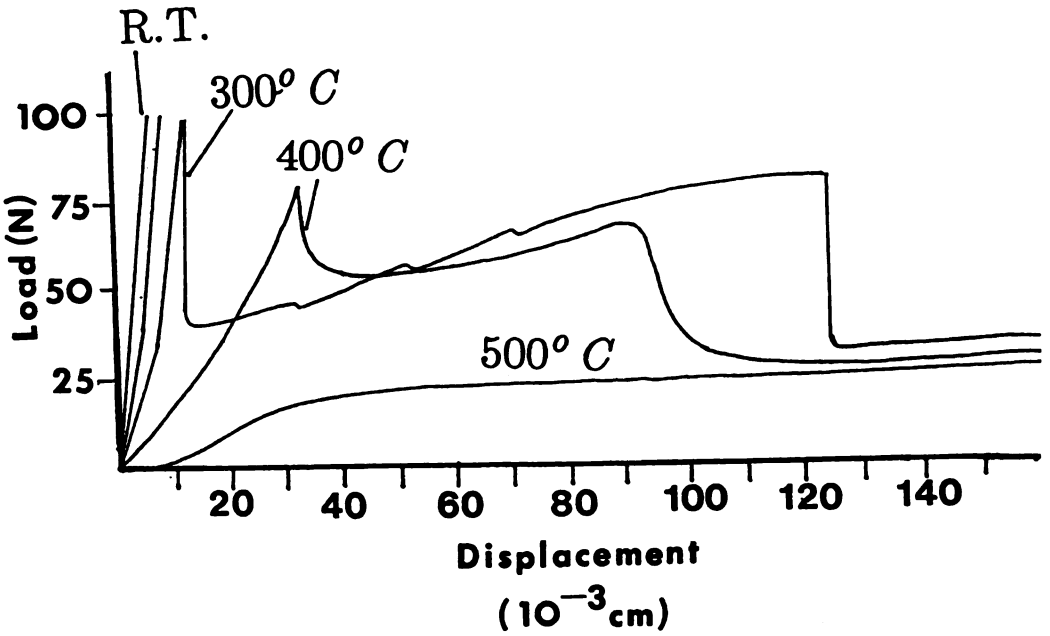


FIGURE 3: The load-displacement curves of the composite specimens ($V_f$=1.25%) at various temperatures.

the composite failed at a very low load.

The observed changes in the load-displacement curves is an indication of the change (decrease) in the ribbon-matrix interfacial bond strength. These changes in the interfacial bond strength (with temperature) also have a significant effect on the load transfer characteristics between the matrix and the ribbons, which in turn affects the failure mode of the composite itself. In order to fully understand this phenomenon, the mechanism of load transfer from the matrix to the ribbon needs to be understood.

The ultimate load bearing capacity of ceramic matrix composites is usually determined by the strength of the reinforcement (since the matrix cracks at a much smaller strain). It is however the onset of matrix cracking which is of significance, because it signifies the onset of permanant damage and loss of protection provided by the matrix against oxidation and corrosion of the reinforcements. Hence the matrix cracking stress is likely to be used as a design stress in future applications. For composite systems in which the reinforcements have the larger failure strain (and stress), the failure mode of the matrix (and hence the composite) is found to depend on the volume fraction of

the reinforcements [9]. For volume fractions of reinforcements smaller than a "critical" volume fraction, single fracture of the matrix is observed. In this case failure of the matrix leads to composite failure, since the reinforcements are unable to carry the load when the matrix cracks. For volume fractions of reinforcements greater than the critical volume fraction, failure of the matrix does not lead to composite failure since the reinforcements can still carry the load. The failure mode of the matrix (and hence the composite) changes to one of multiple fracture. The "critical" volume fraction can be obtained by a simple load balance equation and can be written as

$$V_c = \frac{\sigma_m^*}{\sigma_f^* - \sigma_f' + \sigma_m^*}$$

where, $\sigma_m^*$ is the fracture strength of the matrix
$\sigma_f^*$ is the fracture strength of the ribbon
$\sigma_f'$ is the stress transfered to the ribbons when the matrix cracks.

For large reinforcment strains (exceeding the

matrix failure strain), the matrix is observed to crack into blocks of fixed lengths [10,11]. This length can be obtained by considering the load transfer between the reinforcements (ribbons) and the matrix. For the geometry of the ribbon reinforcements, since the load transfer across the ribbon matrix interface occurs by shear

$$N \tau 2(wx + tx) = \sigma^{*}_{m} A_m$$

where, N is the total number of ribbons(continuous)

$\tau$ is the interfacial shear strength

$\sigma$ is the matrix cracking stress

$A_m$ is the cross sectional area of the matrix

w is the width of the ribbons

t is the thickness of the ribbons, and

x is the length of the blocks into which the matrix cracks(which will be equal to the length of the ribbon initially).

Solving for x,

$$x = \frac{\sigma^{*}_{m} A_m}{2 N \tau (w+t)}$$

Multiplying the numerator and denominator by wt(a constant)

$$x = \frac{\sigma^*_m A_m \, wt}{2 N \tau (w+t) wt}$$

Now, Nwt is the total cross sectional area of the ribbons ($A_r$).

Dividing numerator and denominator by the cross sectional area of the composite ($A_c$),

$$x = \frac{\sigma^*_m (A_m/A_c) wt}{2 \tau (w+t) (A_r/A_c)}$$

Since the composites are continuously reinforced volume fraction is equal to area fraction. Hence

$$x = \frac{V_m \sigma^*_m wt}{V_r 2 \tau (w+t)}$$

Since x is a function of both $\sigma^*_m$ and (for a given volume fraction and ribbon dimensions), the failure mode (single matrix crack or multiple matrix crack) will vary depending on the values of $\sigma^*_m$ and $\tau$.

The results of the pullout tests carried out at

various temperatures are provided in Figure 4. Ribbon pullout was observed only at temperatures exceeding 250°C. The matrix strength measured at various temperatures is also plotted in the same figure. Some of the interesting features that can be observed from this figure are the following: Temperature influences both the matrix strength and interfacial shear strength. While the matrix strength was fairly constant upto 400°C, the interfacial shear strength decreased sharply at about 250°C. In an intermediate range from 300° to 400°, the interfacial shear strength was lower than the matrix strength. At temperatures above 400°C, the matrix strength decreased rapidly while the interfacial shear strength exhibited only a moderate decrease.

These changes lead to changes in the failure mode. Visual observations of the composite specimens revealed that specimens tested at temperatures below 200°C exhibit a single matrix crack in composite failure (Figure 5 a). At 300°C, the failure mode of the matrix change to one of multiple matrix cracking (Figure 5 b). Above 400°C, although the interfacial strength was still decreased, the matrix strength was decreased more rapidly due to matrix creep. Hence the failure mode of the composite changed back to one of a

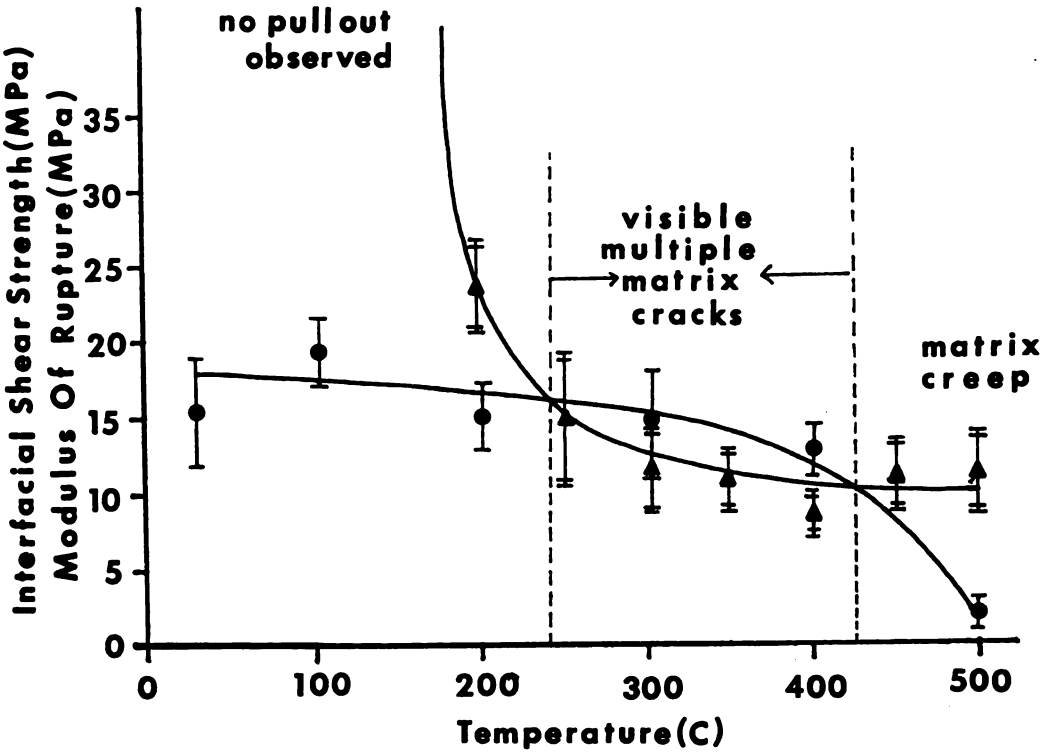


FIGURE 4: The matrix strength and interfacial shear strength at various temperatures.

( ● matrix strength and ▲ interfacial strength)

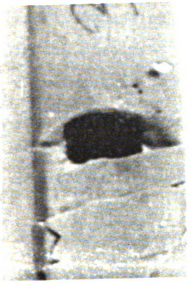

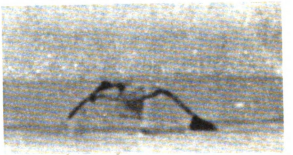

FIGURE 5: Composite failure modes at various temperatures

a. Single crack observed at 200$^{o}$C.

b. Multiple matrix cracks observed at 300$^{o}$C.

c. Single crack observed at 400$^{o}$C.

single crack (Figure 5 c).

The effects of changes in the interfacial shear strength on ribbon pullout can be observed in the scanning electron micrographs provided in Figures 6 and 7. For the specimens tested at temperatures below 300$^{o}$C, no pullout was visible (Figure 6 a and b) and a strong ribbon-matrix interface was observed. At 300$^{o}$C, weakening of the interface was evidenced accompanied by some ribbon sliding (Figure 7 a and b ). The ribbon-matrix debonding and sliding was even more pronounced in the specimens tested at 400$^{o}$C (Figure 8). This ribbon-matrix debonding and sliding provides for additional energy absorption and increased fracture toughness, at temperatures where there is no significant loss of matrix strength.

Hence the metallic-glass reinforcements not only improve the strength and toughness of the glass-ceramic matrices at lower temperatures, but also provide for high temperature toughness by means of interface related effects such as debonding and pullout. Although the metallic-glass ribbon/glass-ceramic matrix combination used in the present study had relatively lower temperature capabilities, proper choice of the matrix and reinforcement could be used to produce

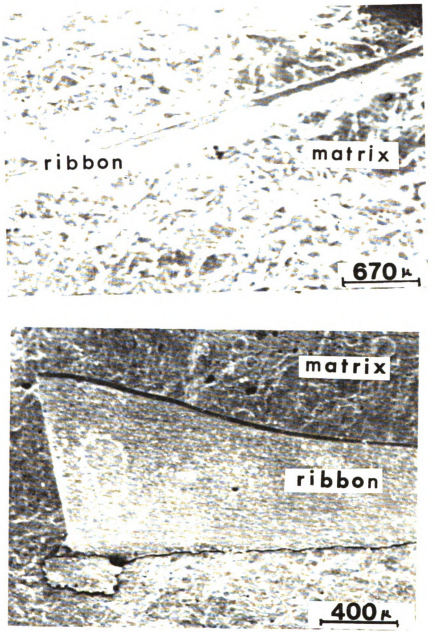


FIGURE 6: Micrographs illustrating the strong interfacial bonding for specimens tested below 300°C.

a. Presence of a strong void free bond between the ribbon and the matrix.

b. Absence of ribbon debonding and pullout.

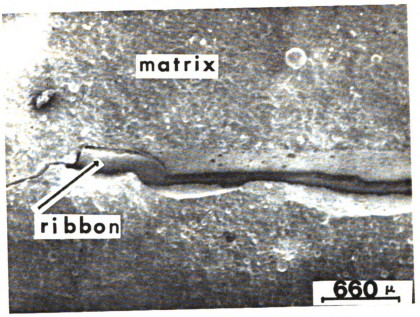


FIGURE 7: Micrographs illustrating ribbon-matrix debonding and ribbon pullout for specimens tested at 300°C.

a. Extensive ribbon debonding and pullout. A crack is observed to initiate at the edge of the ribbon.

b. A high magnification micrograph illustrating the smooth matrix surface in the debonded region.

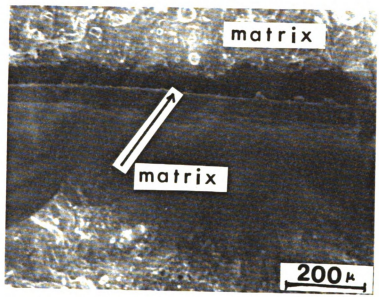


FIGURE 8: Micrograph illustrating extensive ribbon-matrix debonding and ribbon pullout for the specimen tested at 400°C.

composites with high temperature structural capabilities.

**REFERENCES:**


1. Prewo K. M., J. Mater. Sci., 22 (1987) 2695.
2. Luh E. Y. and Evans A. G., J. Am. Ceram. Soc., 70 (1987) 466.
3. Rice R. W., 2 (1978) 69.
4. Sheppard L. M., Adv. Mater. Processes incorporating Metals progress, 130 (1966) 54.
5. Sheppard L. M., Adv. Mater. Processes incorporating Metals progress, 130 (1966) 64.
6. Prewo K. M., Brennan J. J and Layden G. K., Am. Ceram. Soc. Bull., 65 (1986) 305.
7. Vaidya R. U. and Subramanian K. N., J. Mater. Sci., (in press).
8. Vaidya R. U. and Subramanian K. N., ASM/ACCE/ESD Conference Proceedings, Detroit, September 1989 (in press).
9. Hull D., "An introduction to composite materials", edited by Cahn R. W., Thompson M. W. and Ward I. M., Cambridge University press , Cambridge, (1981) pp 125.
10. Aveston J., Cooper G. A. and Kelly A., National Physics Laboratory Conference Proceedings, IPC Science and technology press, Guilford, England, November (1971), pp 15.
11. Marshall D. B. Cox B. N. and Evans A. G., Acta. Metall., 33 (1985) 2013.

# CHAPTER 3

**ABSTRACT:**

A commercially available amorphous metal ribbon incorporated in a glass-ceramic matrix was assessed from the standpoint of fracture toughness. The ribbon orientation (with respect to the long and short transverse sides) relative to the opening crack significantly affected the fracture toughness of such composites. The strong dependance of the fracture toughness on the ribbon orientation was correlated with the differences in the bending contributions of the ribbons in the different orientations. The effect of the ribbon orientation on the crack growth rate in the matrix was also investigated.

## INTRODUCTION:

Studies carried out on metallic-glass ribbon reinforced metal and polymer matrix composites [1-4] have demonstrated some of the unique properties of the ribbon reinforcements. Such composites have been shown to exhibit high longitudional strength coupled with good off-axis properties. Recently, the potential of using such metallic-glass reinforcements for enhancing the mechanical properties of brittle glass-ceramic matrices has been demonstrated [5,6]. Ribbon reinforcements, unlike fiber reinforcements, possess the ribbon width as an additional geometrical parameter. Hence the load transfer characteristics in such ribbon reinforced composites are expected to be influenced by the ribbon width also. Defining the ribbon orientation in such composites is also more involved. In addition to orienting the ribbons with respect to the longitudinal axis of the specimen, the ribbons can also be oriented differently with respect to their long or short transverse faces normal to the opening crack front (The surface bounded by the length and width of the ribbon is referred to as the long transverse face; one that is bounded by the thickness and length is referred to as the short transverse

face). The effect of different ribbon configurations on the fracture toughness of the composites was investigated in this study. An understanding of this effect would be useful in optimizing the properties of such brittle matrix composites, in order to make them suitable for structural applications.

## EXPERIMENTAL PROCEDURE:

Corning glass code 7572 was used as the starting matrix material. METGLAS 2605S-2 was used as the reinforcement. The specimens were fabricated by conventional wet pressing, in a steel die, using amyl acetate as the binder. After compaction (at 3000 Psi), the specimens were preheated to 250$^{o}$C to drive off the organic binder. The compacts were sintered at 400$^{o}$C for one hour followed by a crystallization treatment for 20 minutes. The main crystalline phase is 2PbO.ZnO. Details of the physical properties and chemical compositions of the metallic-glass and glass-ceramic matrix are given elsewhere [6]. The residual stresses induced by the thermal expansion coefficient mismatch between the matrix and the reinforcement can be neglected since $\alpha_{matrix} = 95 \times 10^{-7}$ /$^{o}$C and $\alpha_{ribbon}$ =

76 x $10^{-7}$ /$^{o}$C. Strong bonding was observed between the ribbon and the matrix. The strong nature of the bond was evidenced by the absence of ribbon pullout in the pullout tests conducted [6]. A detailed study of the nature of the bonding and interface characterization is under progress.

Single edge notched beam specimens were used to measure the fracture toughness. The ribbon dimensions used were 4.0 cm x 0.5 cm x 25 microns. The total number of ribbons (and hence the volume percent of the ribbons) was kept the same in all the specimens (at 0.67%). The external dimensions of the composite specimens were also kept constant (4.0 cm x 1.15 cm x 1.20 cm). The notches in the specimens were cut using a slow speed diamond saw. The specimens were annealed at 250$^{o}$C (since the glass-ceramic has a relatively low maximum operating temperature) after the notches were cut, in order to heal any microcracks which might have formed as a result of the machining operations. The various ribbon configurations used are shown in Figure 1. The specimens were tested in three point bending in an Instron machine with a cross head speed of 0.05 cm/min. The bending tests were performed in accordance with A.S.T.M. STP 678 (for blunt notch specimens). Five specimens were tested for each ribbon

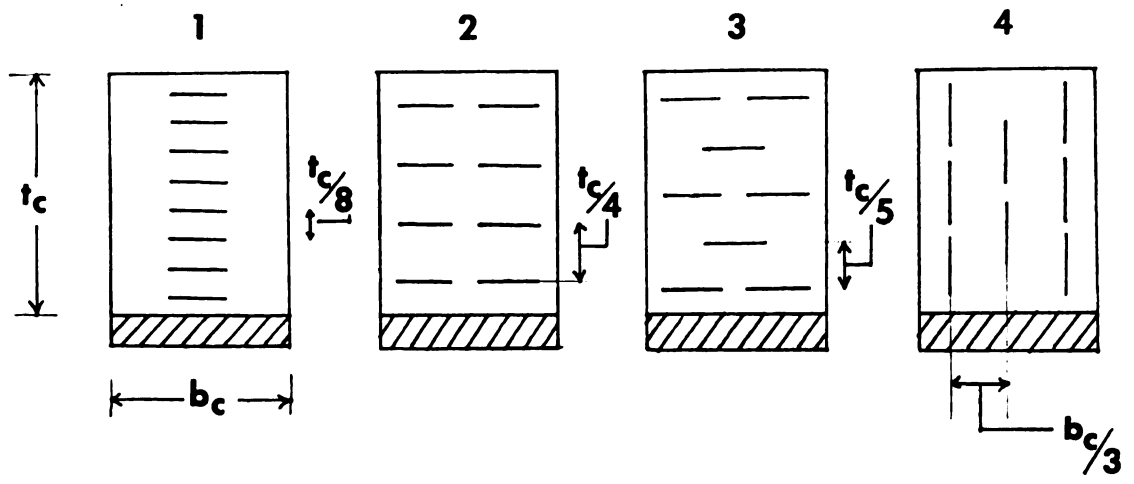


FIGURE 1 : The cross-sectional view of the different ribbon configurations used in the Single Edge Notched Beam specimens. The shaded area represents the notches cut in the specimens.

($b_c$ is the composite width, and $t_c$ is the composite thickness.)

configuration.

## RESULTS AND DISCUSSION:

The measured fracture toughness of the composite specimens (along with the standard deviations) is presented in Table 1. It is evident that the ribbon orientation (with respect to the long and short transverse faces) has a significant effect on the fracture toughness of the composite specimens. The largest increment in the fracture toughness (over that of the matrix) was obtained for ribbons oriented with their short transverse faces perpendicular to the opening crack front (configuration 4 in Figure 1). The differences in the fracture toughness of the composite specimens can be explained on the basis of three important factors.

### a). Ribbon orientation effects:

The primary factor which increases the fracture toughness in configuration 4 (as compared to the other orientations) is believed to be the significantly higher moment of inertia of the ribbons. Consider the

TABLE 1 : Fracture toughness of the composite as a function of ribbon configuration.

| Configuration | $K_{Ic}$ MPam$^{1/2}$ (avg) | Coeff.of Variation (%) |
|---|---|---|
| 0 (Matrix) | 0.321 | 7.07 |
| 1 | 0.683 | 11.52 |
| 2 | 0.987 | 9.79 |
| 3 | 1.161 | 5.00 |
| 4 | 3.177 | 16.50 |

simple case of the bending of a specimen (in three point) containing a single continuous ribbon (lengthwise) located in the center for two different ribbon orientations:

i). Ribbon with its long transverse face parallel to the neutral surface and perpendicular to the opening crack front, and

ii). Ribbon with its short transverse face parallel to the neutral surface and perpendicular to the opening crack front.

The moments of inertia calculated for the orientations i). and ii). are given as $I_i$ and $I_{ii}$ in equations 1 and 2 respectively.

$$I_i = \frac{1}{6} b_f t_f^3 + \frac{1}{3} b_c t_f^3 + \frac{1}{12} b_c t_c^3 \quad \ldots\ldots\ldots (1)$$

$$I_{ii} = \frac{1}{6} t_f b_f^3 + \frac{1}{12} b_c t_c^3 + \frac{1}{4} t_f b_f^2 (t_c - b_f) + \frac{1}{12} t_f (t_c - b_f)^3 \quad \ldots\ldots (2)$$

where,

$b_c$ is the width of the composite specimen

$t_c$ is the thickness of the composite specimen

$b_f$ is the width of the ribbon and,

$t_f$ is the thickness of the ribbon.

It can be shown (for the dimensions of the ribbons used in this study) that the bending moment required to obtain the same maximum flexural stress in a ribbon is about 50 times higher when the ribbons are oriented with their short transverse side perpendicular to the opening crack front as compared to the ribbons oriented with their long transverse sides perpendicular to the opening crack front.

b). Matrix energy absorption effects:

Another factor which contributes to the improved fracture toughness in orientation 4 (as compared to orientations 1, 2 and 3) is the differences in the energies absorbed by the matrix. Ceramic materials can exhibit different fracture features depending on the velocity of the crack [7,8]. The velocity of a crack through a brittle matrix also significanly affects the energy absorbed by the matrix. Broberg [9] has indicated that a substantial increase in the energy dissipation in the plastic region (at the tip of the crack) takes place at low crack velocities, whereas a substantial increase in the energy dissipation in the

process zone occurs at higher crack velocities.

The energy absorbed by the matrix during fracture can be written as [9]

$$G_{cm}b = R_1(b-r_p) + R_2(r_p) \quad \ldots\ldots\ldots\ldots\ldots\ldots (3)$$

where,

$G_{cm}$ is the critical strain energy release rate for the matrix

b is the width of the specimen

$R_1$ is the brittle component of $G_{cm}$

$R_2$ is the ductile component of $G_{cm}$ , and

$r_p$ is the size of the plastic zone.

For the ribbon geometry, this equation can be written as [3]

$$G_{cm} = G_{ms}n(A_s/A) + G_{mr}[1 - n(A_f+A_s)/A] \quad \ldots\ldots (4)$$

where,

$G_{ms}$ is the stable (slow) crack growth component of $G_{cm}$

$G_{mr}$ is the unstable (fast) crack growth component of $G_{cm}$

n is the total number of ribbons

$A_s$ is the area of stable crack growth

$A_f$ is the cross sectional area of a ribbon, and

A is the cross sectional area of the composite

specimen.

Since the energy required for propagating an unstable crack is greater than the energy required for propagating a stable crack in a ceramic material [7,8], one can assume

$$G_{mr} = K\, G_{ms} \quad \text{.....(5)}$$

where, K is a positive constant, greater than one.

Using equation (5), equation (4) can be simplified to a form

$$G_{cm} = G_{ms}[C - D\, A_s] \quad \text{.....(6)}$$

where C and D are positive constants. As per this equation, $G_{cm}$ is inversely proportional to the area of stable crack growth.

Previous studies carried out on brittle ceramic materials [7,8] have indicated that it is possible to distinguish between the areas of stable and unstable crack growth using microscopic techniques. In the case of stable crack growth (in the brittle matrix), the crack has enough time to choose its path, and

propagates along a path of least resistance (usually grain boundaries). Thus the fracture for a specimen in which the crack has grown slowly is predominantly intergranular. In case of unstable (rapid) crack growth, the crack grows in a linear self-similar manner, and the fracture observed in this case is predominantly transgranular.

Fels et al. [3] have considered the effect of ribbon orientation on the velocity of the crack through the matrix. A similar analysis will predict the area of stable crack growth in configuration 4 to be significantly smaller than that in the other three configurations. This is because of the smaller crack front intercepted by the ribbon. The smaller dimension of the ribbon intercepting the rapidly propagating crack front decelerates only a small portion of it. As a result the area of stable crack growth in the matrix, which is located in the vicinity of the ribbon is reduced dramatically. Consequently only a very small portion of the crack front needs to accelerate as it leaves the ribbon to catch up with the rapidly propagating front. In this manner, the fracture behaviour of the matrix, influenced by the presence of the ribbons, also contributes to the increased fracture toughness.

In order to observe the regions of stable and unstable
crack growth in the system under investigation, the composite specimens were lightly etched with a 3% hydroflouric acid solution. Scanning electron micrographs (Figures 2 a and b) obtained for specimens containing ribbons in the two different orientations, reveal some distinctive features. In both cases (ribbon oriented with its short or long transverse surfaces perpendicular to the crack front), the ribbon arrested the rapidly propagating matrix crack. The crack could not bypass the ribbon, because the crack has to intersect the ribbon since it will propagate along a plane perpendicular to the length of the ribbon. Once the crack propagates through the ribbon, it propagates catastrophically (because of the large amount of energy available for its growth) and tries to catch up with the the rest of the crack front that has propagated in regions in which it has not been intercepted by the ribbon. The strong ribbon-matrix interface prevents crack deflection at the interface. The region adjacent to the ribbon indicated the presence of an "intermediate zone" (marked `X'in Figures 2 a and b) , wherein the crack accelerated to catch up with the propagating crack front in the other regions of the matrix. The crack usually initiates at

FIGURE 2:a. Scanning electron micrograph illustrating the fracture features observed for a specimen containing ribbons oriented with their long transverse faces perpendicular to the crack front.

b. Scanning electron micrograph illustrating the stable and unstable crack growth regions in a specimen containing ribbons oriented with their short transverse faces perpendicular to the crack front.

Arrow indicates the direction of crack propagation in the composite. `X' and `Y' correspond to regions of unstable and stable crack growth respectively. `X' corresponds to the intermediate zone referred to in the text.

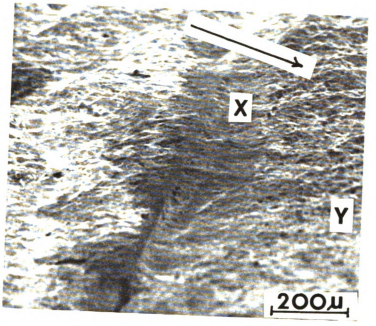
X
Y
200μ

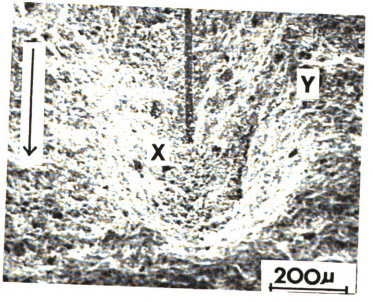
Y
X
200μ

a different level on the far side of the ribbon (probably due to flaws existing at the interface, or due to bending of the ribbon), and accelerates to catch up with the propagating crack front. In doing so, the crack has to climb, thereby traversing a longer and tedious path. However, this region (intermediate zone) appears to be smoother as compared to the surrounding region (marked `Y' in Figures 2 a and b). This indicates that the crack propagates more rapidly in this region. The size of the intermediate zone depended on the ribbon orientation. This zone was relatively larger in the specimens containing ribbons oriented with their short transverse faces perpendicular to the crack front.

This observation is not in agreement with the model of crack growth in such a region proposed by Fels et al. [3] for polymer matrix composites. This is probably as a result of the different magnitudes of interfacial bonding between the component phases. In the case of the system under investigation, the strong bond between the matrix and ribbons prevented any matrix sliding. Hence the crack cannot propagate through the matrix without fracturing the ribbons. In case of the metallic-glass/polymer matrix composite studied by Fels et al. [3], the interface was relatively weak. Hence the crack could propagate

through the matrix without ribbon failure, although at a much slower rate. Similar features were observed in studies on a nichrome ribbon/slide glass system [10], where the interfacial bond strength was relatively low.

c). Ribbon spacing effects:

The differences in the fracture toughnesses measured for configurations 1,2 and 3 could be attributed to the different spacing of the ribbons (since the moments of inertia for all three orientations are the same). The spacing between ribbons in configuration 1 is much smaller than the spacing between ribbons in configurations 2 and 3. Hence, for configuration 1 it is possible that the intermediate zone overlaps with ribbons, thereby absorbing a smaller amount of energy. The differences in the spacing of the ribbons in configurations 2 and 3 is small. In fact configuration 3 has a slightly smaller ribbon spacing as compared to configuration 2, but exhibits a higher $K_{IC}$. This is probably due to the more complex arrangement of the ribbons leading to a larger intermediate zone. In addition, the propagating crack front will be intersected by the ribbons more effectively in this ribbon configuration. Although the

presence of stable and unstable crack growth was detected in the matrix, further studies to quantify the process are essential.

## CONCLUSIONS:

The fracture toughness of continuous metallic-glass reinforced glass-ceramic matrix composites is strongly dependant on the ribbon orientation (long transverse or short transverse faces) with respect to the opening crack front. This was attributed to the differences in the bending moments associated with the different ribbon orientations. The ribbon orientation was affected the crack velocity in the matrix and subsequently the fracture toughness of the composites.

## ACKNOWLEDGEMENTS:

The authors would like to acknowledge the Composite Materials and Structures Center at Michigan State University for supporting and funding this project. The authors would also like to thank Dr. N.

J. Altiero of Michigan State University for his helpful suggestions during the preparation of this manuscript. The authors would also like to extend their sincere thanks to Dr. Kenneth Chyung of Corning Glass Inc. and Dr. Edward Norin of Metglas Products for their valuable help and suggestions during the early stages of this project.

**REFERENCES:**


1. Cytron S. J., "A metallic glass metal matrix composite" J. Mater. Sci. Letters., 1 (1982) 211-13.
2. Strife J. R. and Prewo K. M., "Mechanical behaviour of an amorphous ribbon reinforced resin matrix composite", J. Mater. Sci., 17 (1982) 359-68.
3. Fels A., Friedrich K. and Hornbogen E.,"Reinforcement of a brittle epoxy resin by metallic glass ribbons", J. Mater. Sci. Letters., 3 (1984) 569-74.
4. Friedrich K., Fels A., and Hornbogen E.,"Fatigue and fracture of metallic glass ribbon/epoxy matrix composites", Comp. Sci. and Tech., 23 (1985) 79-96.
5. Vaidya R. U. and Subramanian K. N., "Metallic-glass reinforcement of glass-ceramics" ASM/ACCE/ESD Conference Proceedings, Detroit, Published by American Society of Metals, Metals Park, Ohio (1989) pp 227-231.
6. Vaidya R. U. and Subramanian K. N., "Metallic-glass ribbon reinforced glass-ceramic matrix composites", J. Mater. Sci. (in press).
7. Jessen T. L. and David Lewis III, "Effect of crack velocity on crack resistance in brittle-matrix composites", J. Am. Ceram. Soc., 72[5] (1989) 818-21.
8. Jessen T. L., Mecholsky J. J. and Moore R. H., "Fast and slow fracture in glass composites reinforced with

Fe-Ni-Co alloys", Am. Ceram. Soc. Bull., 65[2] (1986) 377-81.

9. Broberg K. B., "On the effects of plastic flow at fast crack growth" from Fast Fracture and Crack Arrest, ASTM STP 627, edited by Hahn G. T. and Kanninen M. F., American Society for Testing and Materials, 1977 pp 243-56.

10. Vaidya R. U., Lee T. K. and Subramanian K. N., "Metallic ribbon reinforcement of ceramics" ASC Fifth Technical Conference Proceedings. (in press).

# CHAPTER 4

**ABSTRACT:**

The load transfer mechanism in a metallic-glass ribbon reinforced glass-ceramic matrix composite was investigated. The critical ribbon length required for effective load transfer between the matrix and the ribbons, was found to be a function of the ribbon width. This dependance was attributed to the size of the long-transverse side available for load transfer.

**INTRODUCTION:**

Unidirectional fiber reinforcement has been found to be a very effective method for improving the strength of brittle glass and glass-ceramic matrices [1-3]. The major drawback of such unidirectionally reinforced composites is their relatively poor off-axis properties. One of the ways in which this problem has been overcome is in the use of multiple plys, containing fibers oriented at different angles ($0^{o}$, $45^{o}$, $90^{o}$ etc) with respect to the longitudinal axis [4]. Although such composites are isotropic on a macroscopic scale, the properties within each ply are not the same in different directions. This anisotropy within each ply can have serious consequences on the failure mode of such composites.

Ribbon reinforced composite plys have been found to exhibit transverse strengths approaching about 50% of their longitudinal strength. These are achieved because of the unique geometry of the ribbon reinforcements. Metallic-glasses appear to be the best candidates as ribbon reinforcements for the following

reasons. They exhibit very high strength and fracture toughness (far exceeding that of the parent metal from which they are derived). Their ribbon geometries are also a natural consequence of the extremely high cooling rates required in their manufacture. Metallic-glass reinforced polymer and metal matrix composites have been found to exhibit very high strengths [5-7]. Recently, metallic-glass ribbons were investigated as reinforcements for brittle glass-ceramic matrices. Even small volume fractions of such reinforcements improved the mechanical properties of the glass-ceramic matrices quite significantly [8].

The geometry of the ribbons is significantly different from that of conventional fibers, and as a result the load transfer characteristics are expected to differ from those related to fiber reinforced systems. An understanding of this feature is important for structural applications of ribbon reinforced composites. The present study addresses some of the aspects of load transfer in a metallic-glass ribbon reinforced glass-ceramic matrix composite.

**THEORY:**

In the case of metallic-glass reinforced glass-ceramics, where both the failure stress and failure strain of the reinforcement exceed that of the matrix, the composite strength can be expressed by

$$\sigma_c^* = \sigma_m^* V_m + \sigma_f' V_f \quad \text{for} \quad V_f < V_c \quad \ldots\ldots\ldots(1)$$

and $$\sigma_c^* = \sigma_f^* V_f \quad \text{for } V_f > V_c \quad \ldots\ldots\ldots(2)$$

where, $\sigma_c^*$ is the composite fracture strength

$\sigma_m^*$ is the matrix fracture strength

$\sigma_f^*$ is the ribbon fracture strength

$\sigma_f'$ is the stress in the ribbons when the matrix is about to fracture

$V_f$ is the volume fraction of the ribbons

$V_m$ is the volume fraction of the matrix , and

$V_c$ is the "critical volume fraction" of the ribbons.

The "critical volume fraction" is the minimum volume fraction of reinforcements required for preventing the catastrophic failure of the composite when the matrix fractures. It can be obtained by combining equations 1 and 2.

Hence,

$$V_c = \frac{\sigma_m^*}{\sigma_f^* - \sigma_f' + \sigma_m^*} \quad \text{.....(3)}$$

For the system used in this investigation, $\sigma_m^*$ = 15 MPa $\sigma_f^*$ = 700 MPa and $\sigma_f'$ = 685 MPa. The critical volume fraction for the given system was determined using these values and was found to be 0.5%.

When the composite is loaded, the failure strain of the matrix is reached first and it cracks. The load is transferred to the ribbons by shear across the interface. Hence,

$$\sigma_m^* A_m = 2\tau (wx + xt) \quad \text{.....(4)}$$

where, $\tau$ is the interfacial shear strength

$A_m$ is the total area of the matrix.

x is the ribbon length

w is the ribbon width, and

t is the ribbon thickness.

This equation can be rewritten in terms of the volume fractions of the ribbons and the matrix as

$$\sigma_m^* V_m = \frac{2\tau (wx + xt) V_f}{wt} \qquad \text{.....(5)}$$

For the system under investigation, the Young's modulus of the ribbons is greater than that of the matrix ($E_{ribbon}$ = 85 GPa and $E_{matrix}$ = 33 GPa).

In the initial stages of loading (for a volume fraction of reinforcements greater than the critical volume fraction), the load is carried by the matrix and the ribbons. When the failure strain of the matrix is reached, the matrix fails and the load is transferred to the ribbons. The ribbons continue to carry the load till failure.

The maximum strength of the composite is reached if the ribbon length is greater than a critical length $\ell_c$ when $\sigma_f = \sigma_f^*$. Hence (for $x = \ell_c$) the maximum composite strength is

$$\sigma_c^* = \sigma_f^* V_f = \frac{2\tau V_f (w + t) \ell_c}{wt} \qquad \text{.....(6)}$$

## EXPERIMENTAL PROCEDURE:

In order to determine the critical load transfer length, ribbons of varying lengths and three different widths (0.2, 0.5 and 0.8 cm) were incorporated in the glass-ceramic matrix. The specimen length ( 4.0 cm), the specimen width ( 1.0 cm) and the volume fraction of the ribbons (0.67%-greater than the critical volume fraction) were maintained constant for all the specimens.

Metglas 2605S-2 was used as the reinforcement. Corning glass code 7572 was used as the starting matrix material. The specimens were fabricated by conventional wet pressing, using amyl acetate as the binder in a steel die with a pressure of 3000 Psi. After compaction, the specimens were preheated to 250$^{o}$C to drive off the organic binder and then sintered at 400$^{o}$C for one hour. The crystallization of the matrix was achieved by holding the composite at 450$^{o}$C for 20 minutes. Details of the physical and chemical properties of the metallic-glass reinforcement and glass matrix used are given elsewhere [8]. Residual stresses induced by the thermal expansion coefficient mismatch between the matrix and reinforcement ( $\alpha_{matrix}$ = 95 x $10^{-7}$/ $^{o}$C and $\alpha_{ribbon}$ = 76 x $10^{-7}$/ $^{o}$C) can be

considered to be negligible.

Due to the difficulties encountered in gripping of tensile specimens, the strength of ceramics is normally evaluated using bending tests. The maximum outer fiber stress (usually expressed as the Modulus of Rupture, MOR) is taken as a measure of strength. In the present study, tests were carried out in three point bending in accordance with ASTM standard No. C-203/85. All the specimens were carefully polished (using 0.03 micron alumina powder) before testing in order to minimize the effect of surface flaws. A total of five specimens were tested to obtain the average value for each data point. In all the specimens, the failure occurred at the midpoint, which experiences the maximum bending moment.

## RESULTS AND DISCUSSION:

The variation in the strength of the composite specimens as a function of ribbon lengths, for three different ribbon widths are shown in Figure 1. Similar trends have also been observed in other fiber reinforced systems [9].

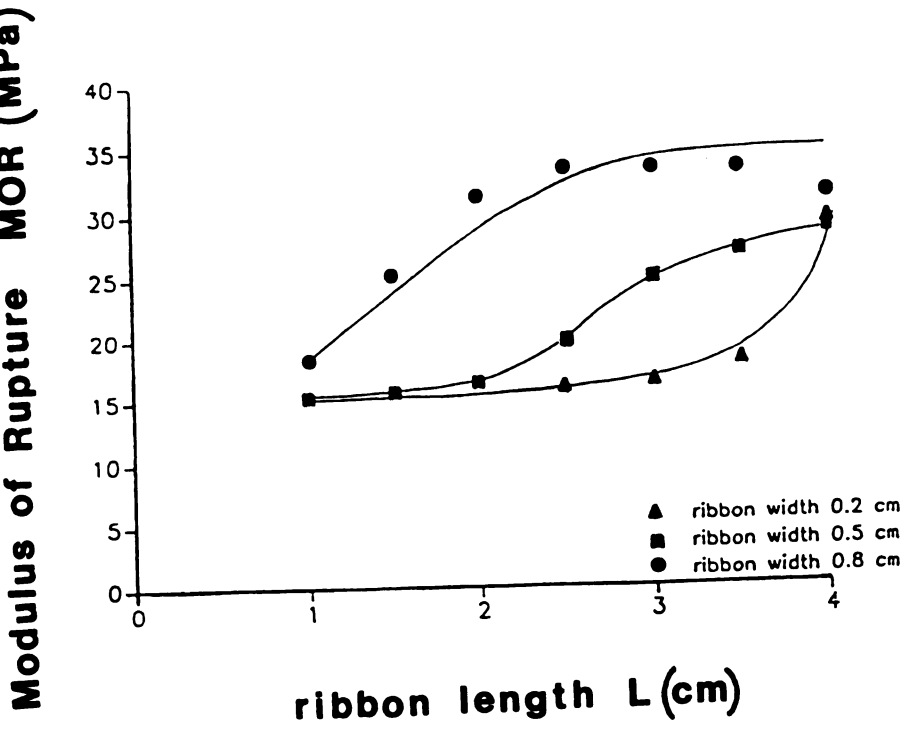


FIGURE 1: Variation in the composite fracture strength as a function of ribbon length.

Increasing the ribbon length enhances the load transfer upto a certain "critical" ribbon length. Increasing the length of the ribbon beyond this "critical" length does not improve the composite strength. For a critical ribbon length $\ell_c$, corresponding to a ribbon width of 0.8 cm (the maximum based on experimental limitations), the composite strength can be approximated by the equation

$$\sigma_c^* = \frac{2\tau V_f(w + t)}{wt} \ell_c \exp[-(\ell_c - x)/x] + (\sigma_m^* V_m) \quad \ldots . (7)$$

where the exponential factor accounts for the load carrying capacity of the composite for ribbon lengths in the range of $0 < X < \ell_c$. This exponential factor was obtained by emperical curve fitting. This equation satisfies the boundary conditions. When $x = 0$, the ribbon contribution is zero and the composite strength is equal to the matrix strength. For $x = \ell_c$ (critical length), the composite strength is a maximum as given by equation 6.

Studies carried out on other metallic-glass ribbon reinforced systems (polymer matrices) [7], have

assumed the load transfer from the matrix to the reinforcing ribbons to be linear. According to this study, the composite strength can be given by

$$\sigma_c^* = \sigma_f^* V_f (1 - \ell_t/\ell) + (\sigma_m^* V_m) \quad \ldots\ldots\ldots\ldots (8)$$

where $\ell$ is the ribbon length and $\ell_t$ is the critical transfer length. However, the experimental findings for the system under investigation did not agree with this equation. In addition, this equation can only be used to predict composite strengths for ribbon lengths in the range $0 < \ell < \ell_t$. It does not satisfy either of the limiting conditions (at $\ell = 0$, $\sigma_c^* = \sigma_m^* V_m$ and at $\ell = \ell_t$, $\sigma_c^* = \sigma_f^* V_f$)

Since the thickness of the ribbon is very small as compared to its width, (w + t) can be approximated to `w'. Hence equation 7 can be simplified to

$$\sigma_c^* = \frac{2\tau V_f \ell_c}{t} \exp[-(\ell_c - x)/x] + (\sigma_m^* V_m) \quad \ldots\ldots (9)$$

Taking the logarithms of both sides of equation 9 and simplifying

$$\ln(\sigma_c^* - \sigma_m^* V_m) = K - \ell_c/x \quad \ldots\ldots\ldots\ldots (10)$$

where K is a positive constant.

A plot of $\ln(\sigma_c^* - \sigma_m^* V_m)$ versus $X^{-1}$ is shown in Figure 2. The slope of this line is the critical length $\ell_c$, which was found to be 2.581 cm.

Although the equations described were developed for a ribbon width of 0.8 cm, the same equation can be used for composites containing ribbons of other widths, provided a geometrical correction factor is applied. This correction factor can be referred to as the "shift factor".

The concept of "shift factor" can be understood by considering the experimentally obtained data of the composite strength as a function of ribbon length (Figure 1). This strength data can be replotted against the ribbon length to width ratio (Figure 3). The strength curve appears to shift depending on the ribbon width when plotted against the ribbon length to width ratio. The curve corresponding to a ribbon width of 0.8 cm was chosen as the master curve. All the data corresponding to the other ribbon widths can be shifted onto this master curve by using the "shift factor".

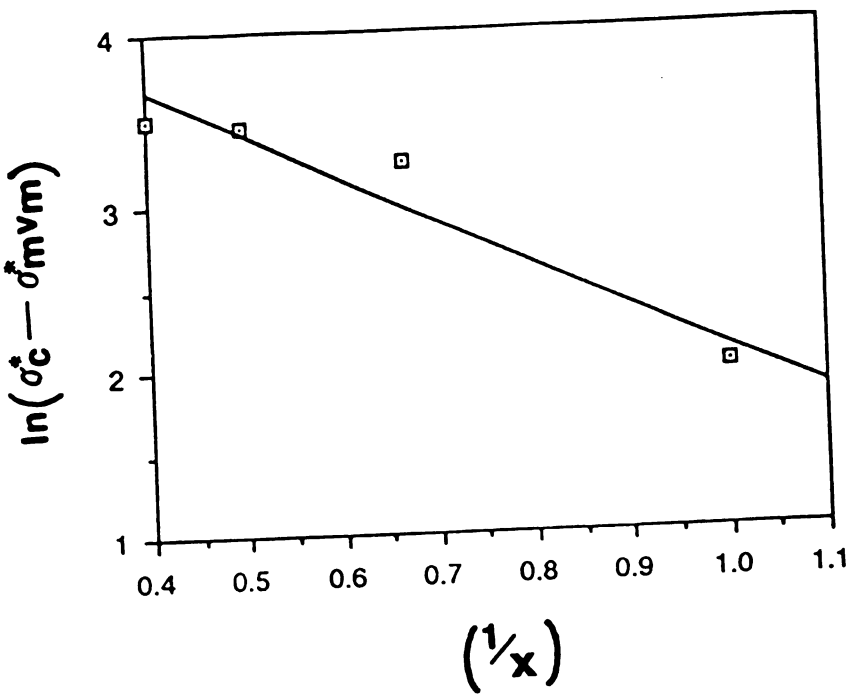


FIGURE 2: Variation in the composite fracture strength as a function of reciprocal ribbon length. Strength is expressed in MPa, and reciprocal length is expressed in $(cm)^{-1}$.

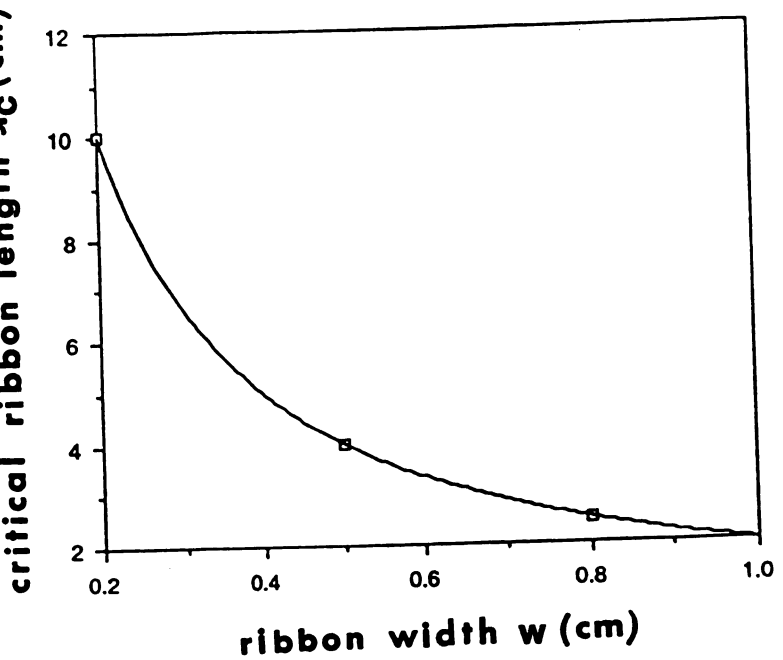


FIGURE 3: Variation in the critical ribbon length as a function of ribbon width.

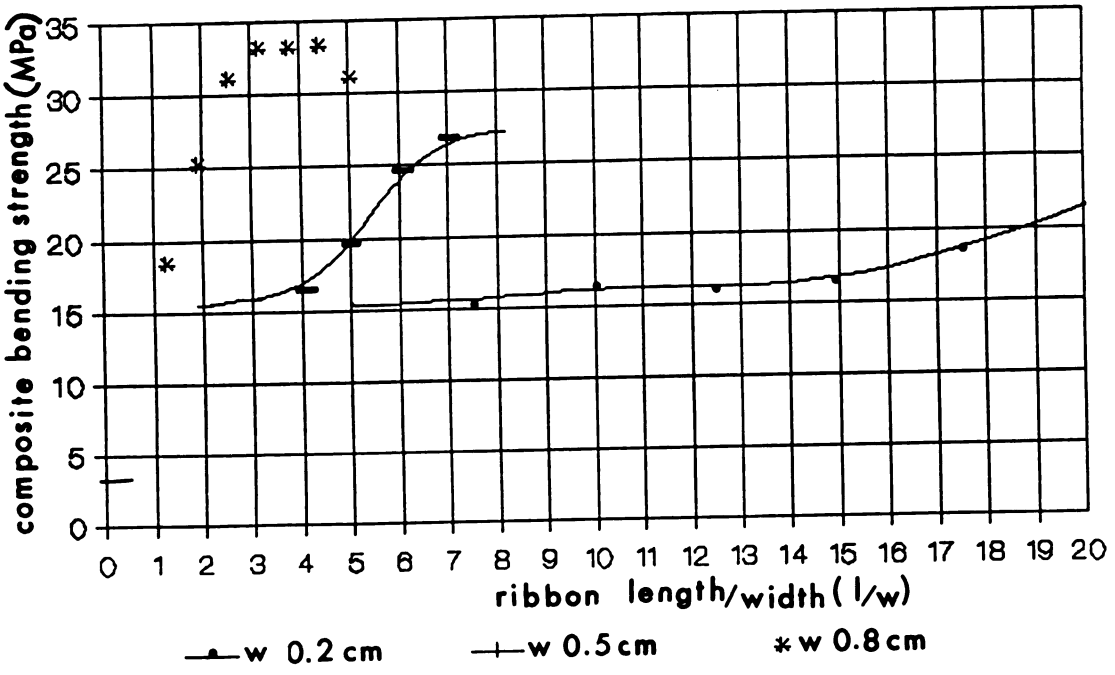


FIGURE 4 : Variation in the composite bending strength with the ribbon length to width ratio.

The shift factor "a" can be defined as

$$a = \frac{\text{length of ribbon required to obtain a given strength in a composite containing ribbons of width 0.8 cm}}{\text{length of ribbon required to obtain the same strength in a composite containing ribbons of width other than 0.8 cm}}$$

According to this definition

$a = 1$ for a ribbon width of 0.8 cm, and
$a > 1$ for a ribbon width less than 0.8 cm.

Values of the shift factor can be obtained from the plot of the strength versus the ribbon length to width ratio (Figure 3). Variation in the reciprocal shift factor with ribbon width is shown in Figure 4.

The shift factors can now be used to shift all the data corresponding to various ribbon widths onto a single master curve (Figure 5), facilitating the use of the earlier proposed equations for the composite strength.

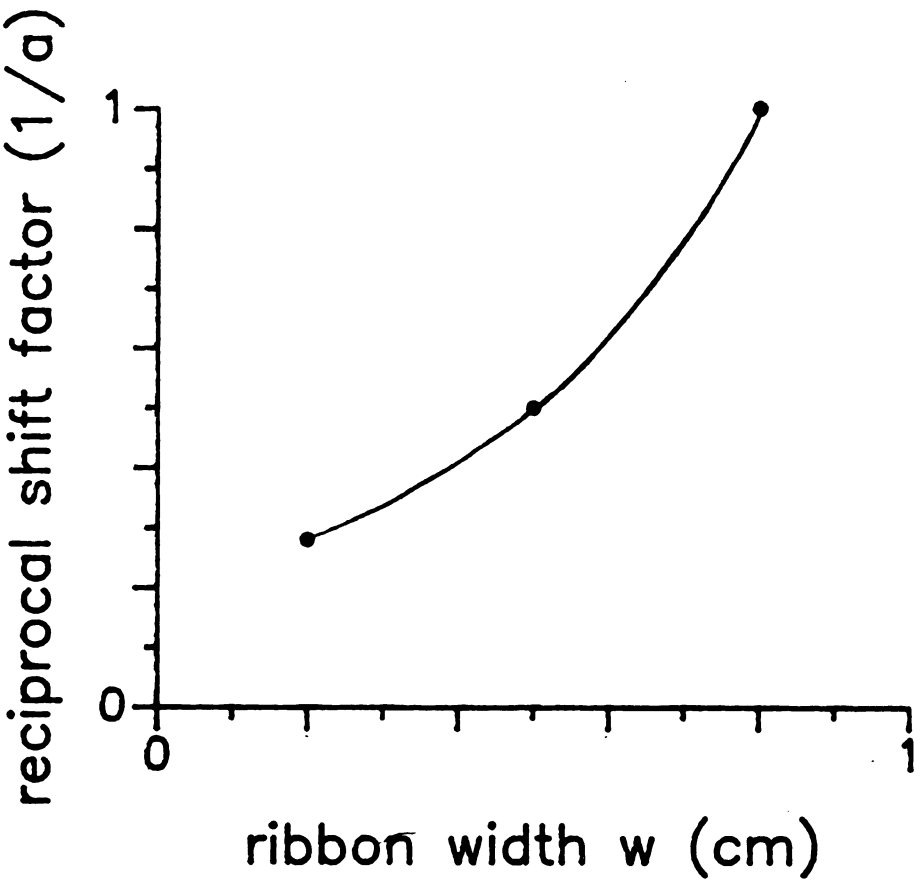


FIGURE 5: Variation in the reciprocal shift factor with ribbon width.

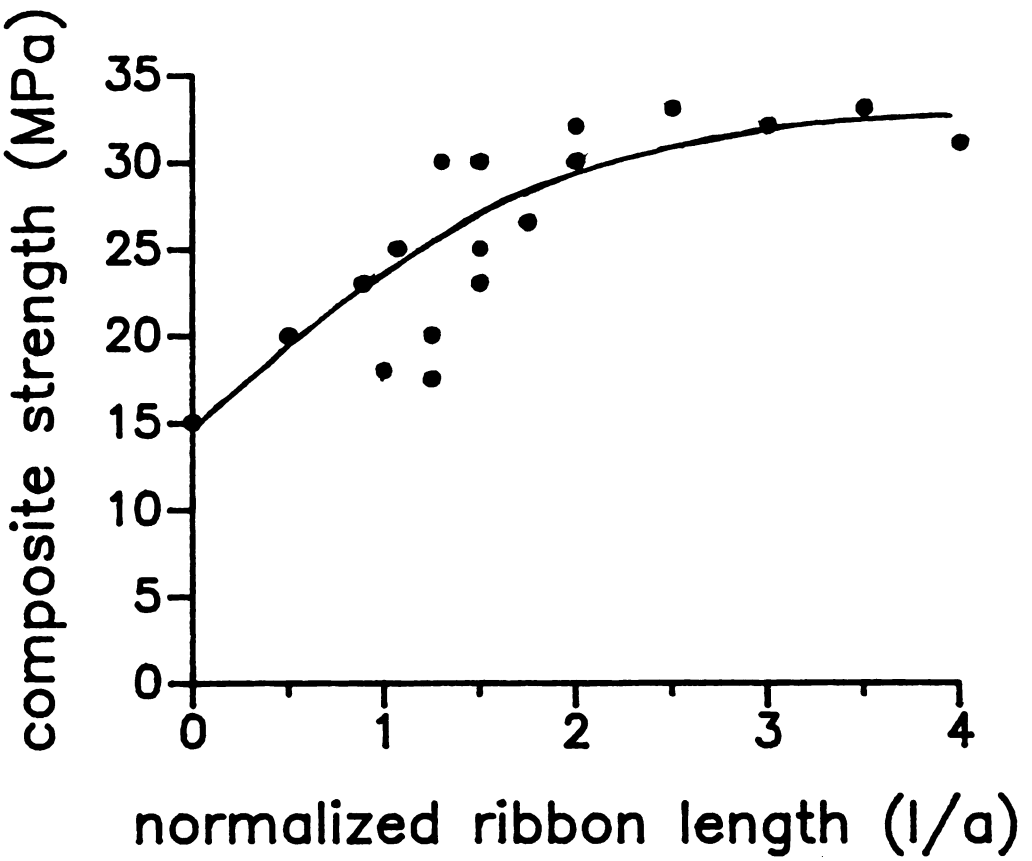


FIGURE 6 : Variation in the composite bending strength with normalized ribbon length.

The ribbon width was found to have a significant effect on the load transfer between the ribbon and the matrix. A plot of the variation in the critical length as a function of ribbon width is shown in Figure 6. This effect is probably a consequence of the non-uniform bending moment along the specimen and hence the non-uniform stress in the cross-section experienced by the composite specimen in the bend test. In the three point bending configuration the bending moment is a maximum in the center of the specimen and drops of to zero at the specimen ends. The specimen failure is usually initiated in a region close to where the maximum bending moment (and hence the maximum outer fiber tensile stress) is encountered. The effective ribbon area encountered by a crack decreases as the ribbon width decreases. This ribbon area is critical because stress transfer occurs from the matrix to the ribbon across this area. This explains the larger critical lengths observed for the specimens with the smaller width reinforcements.

Another factor which localizes the stress to a very small region in the matrix is the presence of an extremely strong bond between the ribbon and the matrix. The nature of the bonding between the matrix and the reinforcements can be seen in Figures 7 a and

FIGURE 7: Micrographs illustrating the nature of the bonding between the glass-ceramic matrix and the metallic-glass ribbon reinforcement.

a. Absence of ribbon pullout in a pullout test.

b. Presence of a strong void-free bond between the ribbon and the reinforcement.

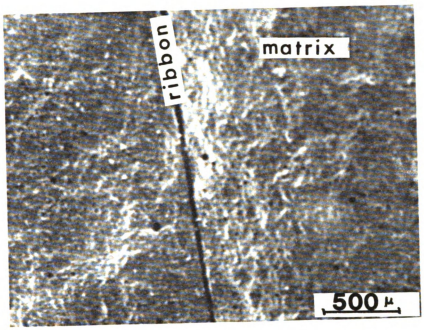
ribbon
matrix
500 μ

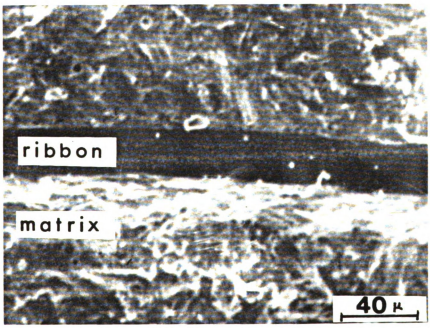
ribbon
matrix
40 μ

b. According to the ACK theory [10], the interfacial strength between the reinforcement and matrix controls the load transfer across the interface and also affects the load transfer length. The load transfer length can be obtained by rearranging equation 5 and solving for 'x'. Hence,

$$x = \frac{\sigma_m^* V_m \quad wt}{2 \tau V_f (w + t)} \qquad \text{.....(11)}$$

According to this equation a strong interface results in the load being transferred across a very narrow region in the center of the specimen.

Conclusively it can be said that the load transfer in ribbon reinforced composites cannot be characterized by a simple aspect ratio of length to thickness as considered with other fiber reinforced systems. Specifying the width in such composites is essential, since it affects the load transfer between the matrix and the ribbons quite significantly.

## CONCLUSIONS:

The present study indicates that the load tranfer characteristics in ribbon reinforced composites differ from those in fiber reinforced systems. It is not possible to characterize the load transfer in such composites by a simple aspect ratio ($\ell$/d) as in fiber reinforced systems. The width of the ribbon plays a significant role in the load transfer process. The interfacial bond strength is also found to significantly affect this dependancy. Further studies are needed to completely characterize this behaviour.

**ACKNOWLEDGEMENTS:**

The authors would like to acknowledge the Composite Materials and Structures Center at Michigan State University for funding and supporting this project.

**REFERENCES:**


1. Fitzer E. and Gadow R., Am. Ceram. Soc. Bull., 65 (1986) 326.
2. Herron M. and Risbud S., Am. Ceram. Soc. Bull., 65 (1986) 342.
3. Prewo K. M., Am. Ceram. Soc. Bull., 65 (1986) 395.
4. Ko F., Am. Ceram. Soc. Bull., 68 (1989) 401.
5. Cytron S. J., J. Mater. Sci. Letters, 1 (1982) 211.
6. Strife J. R. and Prewo K. M., J. Mater. Sci., 17 (1982) 359.
7. Strife J. R. and Prewo K. M., **AFWAL Report AFWAL-TR-80-4060,** 1980.
8. Vaidya R. U. and Subramanian K. N., J. Mater. Sci., (in press).
9. Hancock P. and Cuthbertson R. C., J. Mater. Sci., 5 (1970) 762.
10. Aveston J., Cooper G. A. and Kelly A., **National Physics Laboratory Conference Proceedings,** IPC Science and Technology Press, Guildford, England, November 1971, pp 15.

# CHAPTER 5

**ABSTRACT:**

Discontinuous metallic-glass ribbons of varying lengths and widths were used to reinforce a brittle glass-ceramic matrix. The fracture strength and toughness of such composites as a function of ribbon volume fraction and geometry were measured in three point bending. The mechanical properties were found to be relatively isotropic in the plane of compaction (without significant loss of strengthening achieved with unidirectional reinforcement). The higher composite strength exhibited in a direction perpendicular to the plane of compaction was attributed to the higher percentage of ribbons oriented with their short transverse faces perpendicular to the opening crack front.

## INTRODUCTION:

The potential of using metallic-glass ribbons as reinforcements for brittle glass-ceramic matrices has been demonstrated [1-5]. Such composites were produced by relatively simple, and cost effective pressing and sintering techniques. The studies carried out so far have indicated that significant improvements in the mechanical properties of the glass-ceramic matrices can be achieved by the use of relatively small volume fractions of metallic-glass ribbon reinforcements.

Some of the advantages of metallic-glasses which make them attractive as reinforcements is their high strength, toughness and corrosion resistance. The high cooling rates required in their manufacture imparts the ribbon geometry. This ribbon geometry not only provides for a large surface area to bond with the matrix, but has also been found to be useful in improving the off-axis properties, when used as reinforcements for brittle polymer matrix composites [6,7].

The studies carried out so far [1-5] have focused on the reinforcement of brittle glass-ceramic

matrices with continuous metallic-glass ribbon reinforcements. However, these continuously reinforced composites are unsuitable for structural applications, because of the high degree of directional strengthening they provide. Most structural applications demand a good degree of strength isotropy. Fabrication of these continuously reinforced composites is relatively difficult (since they involve ribbon lay up etc). The extremely small thickness of the ribbons also makes it difficult to incorporate large volume fractions of reinforcements into the matrix. In order to overcome these problems, discontinuously reinforced metallic-glass ribbon/glass-ceramic matrix composites were fabricated. The mechanical properties of these composites were measured and compared with those of continuously reinforced composites. The load transfer behaviour in such composites was also studied, and compared to the theoretical model proposed earlier [8].

## EXPERIMENTAL PROCEDURE:

Corning glass 7572 and METGLAS 2605S-2 were used as the matrix and reinforcement respectively. Details of the physical properties and chemical Compositions of the matrix and reinforcement are

provided elsewhere [1].

Three different ribbon dimensions were used in the study viz. 0.5 cm x 0.5 cm (length x width), 1.0 cm x 0.5 cm and 1.0 cm x 0.25 cm. The ribbon thickness was kept constant (25 micrometers). The ribbons were precoated with the glass powder prior to composite fabrication. The precoated reinforcements were mixed with the glass powder (containing 8-10% by weight of amyl acetate binder). The ribbons were distributed as randomly as possible so as to prevent the ribbons from orienting preferentially with respect to one particular face (Figure 1). Pressing was carried out at 3000 psi in a steel die. After compaction, the specimens were heated to 250$^{o}$C for 4-5 hours to drive off the organic binder. Sintering was carried out at 400$^{o}$C for 3 hours and was followed by a crystallization step at 450$^{o}$C for 30 minutes in order to convert the matrix into a glass-ceramic.

The specimens were cut from the fabricated rectangular bars, and were tested in three point bending in an Instron machine, using a cross-head speed of 0.05 cm/min. The three point bend tests were carried out in accordance with ASTM Standard C-203/85. Fracture toughness measurements were carried out using

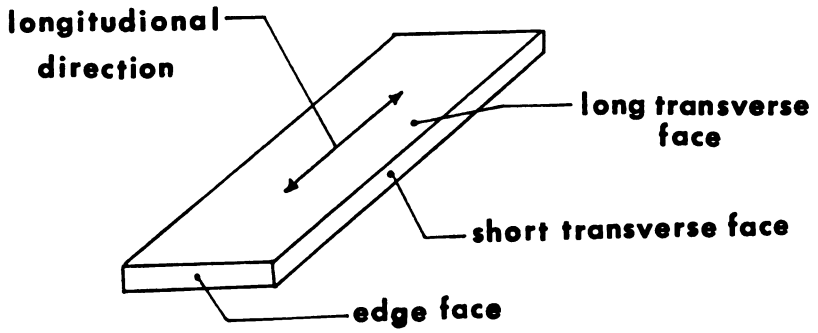


FIGURE 1: Illustration of a ribbon reinforcement indicating the terminology used to represent the various surfaces and directions.

Single Edge Notched Beam specimens (in three point bending). The tests were carried out in accordance with ASTM STP 678. A total of three to five specimens were used to obtain the average value for each data point. In all the specimens failure occurred at the midpoint.

## RESULTS AND DISCUSSION:

The results of the experimentally measured bending strength as a function of increasing volume fraction of reinforcements (for different ribbon dimensions) are given in Table 1. From the data it is evident that increasing the volume fraction of reinforcements increases the strength. The experimentally measured strength of the discontinuous composites was about 80% of the strength of the continuously reinforced composite having the same volume fraction of reinforcements. The strength of the discontinuously reinforced composites can be compared to the theoretical composite strength (continuously reinforced) in Figure 2.

The strength of the composite was measured in three different directions; longitudional denoted by

TABLE 1: Experimentally measured composite strength as a function of ribbon volume fraction, for three different ribbon dimensions.

| Volume fraction of ribbons (%) | Ribbon dimensions length l (cm) | width w (cm) | (l/w) | Average Composite fracture strength (MPa) | Coeff.of Variation (%) |
|---|---|---|---|---|---|
| 5.8 | 0.5 | 0.5 | 1 | 127.75 | 6.8 |
| 5.8 | 1.0 | 0.5 | 2 | 141.99 | 8.4 |
| 5.8 | 4.0* | 0.5 | 8 | 162.4 | |
| 5.8 | 1.0 | 0.25 | 4 | 132.12 | 10.5 |
| 3.5 | 0.5 | 0.5 | 1 | 91.5 | 3.7 |
| 3.5 | 4.0* | 0.5 | 8 | 98.0 | |
| 2.5 | 0.5 | 0.5 | 1 | 58.37 | 2.7 |
| 2.5 | 1.0 | 0.5 | 2 | 73.41 | 6.9 |
| 2.5 | 4.0* | 0.5 | 8 | 70.0 | |
| 2.0 | 0.5 | 0.5 | 1 | 47.18 | 5.5 |
| 2.0 | 4.0* | 0.5 | 8 | 56.0 | |
| 2.0 | 1.0 | 0.25 | 4 | 55.0 | 11.8 |

* indicates ribbon length for a continuously reinforced composite, based on maximum die size.

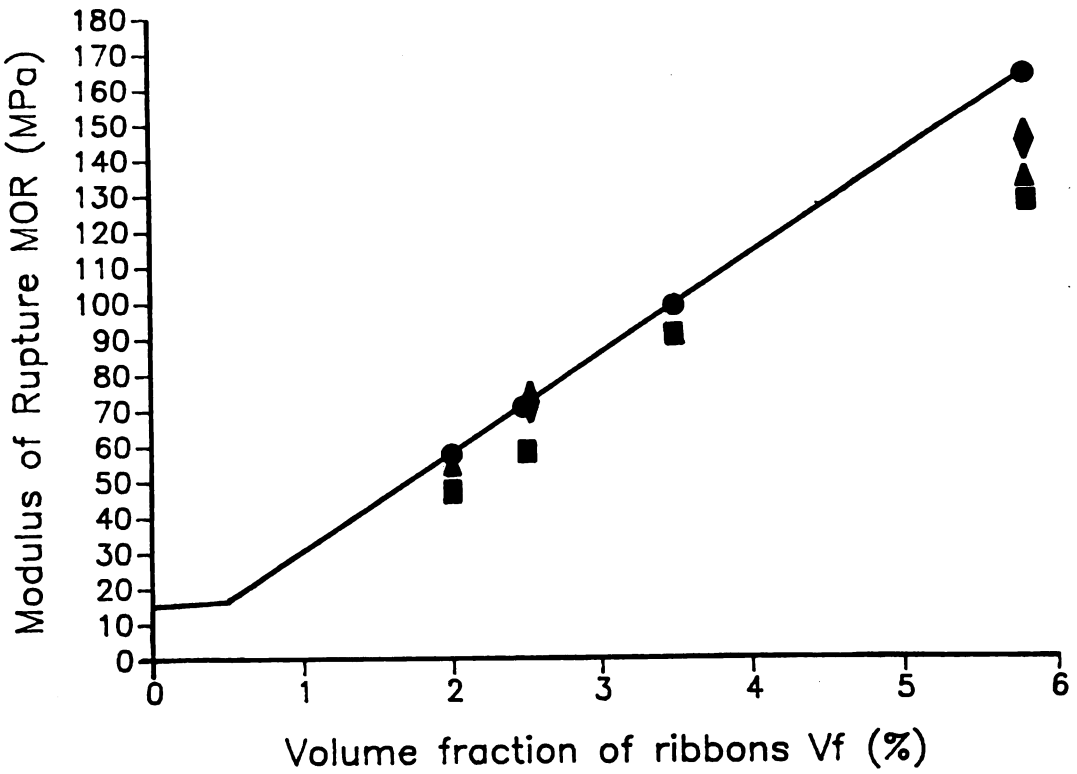
Modulus of Rupture MOR (MPa)
180
170
160
150
140
130
120
110
100
90
80
70
60
50
40
30
20
10
0
0
1
2
3
4
5
6
Volume fraction of ribbons Vf (%)

FIGURE 2: Plot of the composite bending strength as a function of increasing volume fraction of metallic-glass reinforcements.
The solid line drawn through (●) indicates the theoretically predicted composite strength (using $\sigma_c^* = \sigma_f^* V_f$). The other legends represent three different ribbon dimensions as

(■) length 0.5 cm, width 0.5 cm

(▲) length 1.0 cm, width 0.5 cm

(◆) length 1.0 cm, width 0.25 cm.

Ribbon thickness was 25 micrometres.

`L', transverse denoted by `T' and in a direction perpendicular to the plane of compaction denoted by `CT'. These three orientations are shown in Figure 3. All the specimens were cut from the same block of composite material in order to avoid any discrepancies induced due to processing. The strength values obtained for the three different orientations are given in Table 2. The strength of the composite in the transverse direction (T) is about 95% of that in the longitudional direction (L), which in turn is about 80% of the strength of a continuously reinforced composite in the longitudional direction. From the strength values given in Table 2 it is evident that the composite exhibits strength isotropy in the plane of compaction. These results are illustrative of the advantages provided by ribbon reinforcements over fibers. Continuous fiber reinforced composites are extremely weak in the transverse direction (5-25% of the longitudional strength). This drawback is overcome by using multiple plies (containing ribbons oriented in different directions), but at the expense of a reduction in the strength in the longitudional direction. On the other hand, continuous ribbon reinforced composites have been shown to exhibit transverse strengths as high as 50 % of their longitudional strengths [7]. By using discontinuous

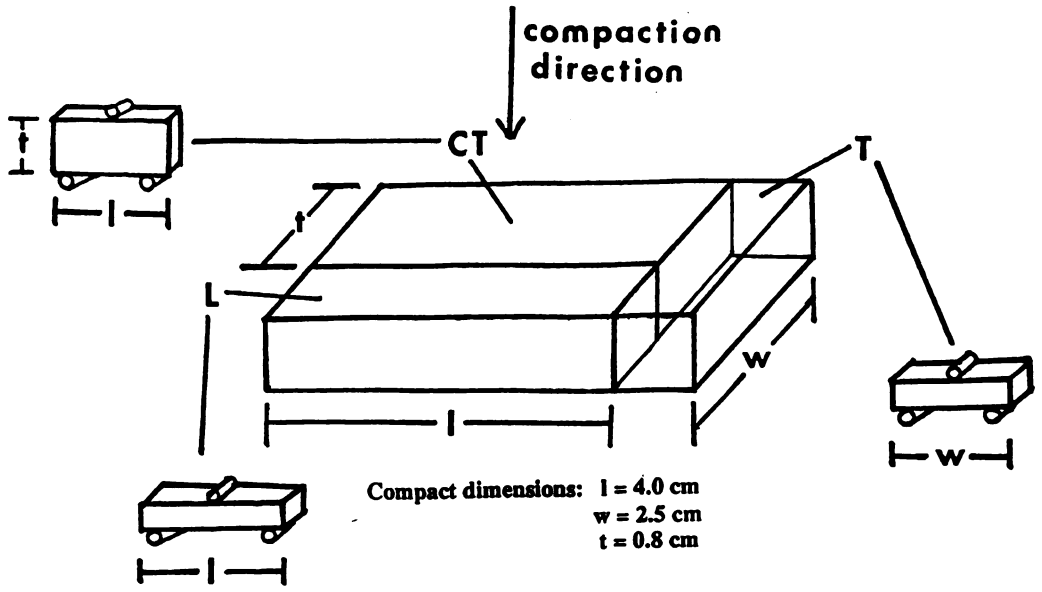


FIGURE 3: Figure illustrating the various orientations in which the composite specimen was tested.

TABLE 2: Experimentally measured composite strength in three different directions. The three directions used are identified in Figure 2.

Volume fraction of ribbons 5.8%

Dimensions of ribbons length 0.5 cm
width 0.5 cm
thickness 25 micrometers

Theoretical composite strength 162.4 MPa

| Direction | Average Composite fracture strength (MPa) | Coeff.of Variation (%) |
|---|---|---|
| L | 132.3 | 5.8 |
| T | 125.8 | 10.1 |
| CT | 146.2 | 3.8 |

ribbon reinforcements of appropriate dimensions, an even higher degree of strength isotropy can be obtained.

In addition to the ribbon geometry, the strength of the bond between the ribbon and the matrix is also significant. Studies carried out on metallic-glass ribbon/polymer matrix composites (which exhibit relatively weak interfacial bonding) [6,7], and Nichrome ribbon/slide glass matrix composites [5] have indicated a lower degree of strength isotropy as compared to the system investigated. Pullout tests carried out on the metallic-glass/glass-ceramic system have indicated the presence of a very strong bond between the matrix and the ribbons. The nature of this bond can be observed in Figure 4. This strong nature of the bond is primarily responsible for the high level of strength utilization of the metallic-glass ribbons, and also the isotropy in the system.

Thus the high transverse strength and in-plane isotropy in such metallic-glass ribbon/glass-ceramic matrix composites can be attributed to three important factors:

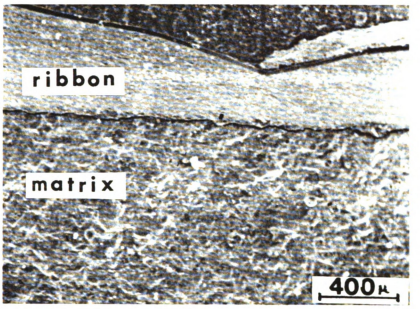


FIGURE 4: Scanning micrograph illustrating the strong bond between the matrix and the ribbon.

1. High strength of the metallic-glass ribbons
2. Unique ribbon geometry, and
3. Good bonding between the metallic-glass ribbons and the matrix.

Specimens with the `CT' configuration exhibited the maximum strength. Although the ribbons were distributed as randomly as possible, a larger fraction of the ribbons reoriented themselves with their long transverse faces (Figure 1) perpendicular to the direction of compaction during the compaction and/or sintering stage. Scanning microscopy carried out on the fractured surfaces confirm this effect (Figure 5). The higher strength obtained for this orientation can be primarily attributed to the higher moment of inertia of the ribbons in that orientation. Details of the orientation effects in such metallic-glass ribbon/glass-ceramic matrix systems have been discussed elsewhere [4,5].

The results of the fracture toughness tests carried out are presented in Table 3. The fracture toughness of the composite specimens was significantly isotropic (though slightly lower in the transverse direction), and could possibly be attributed to the

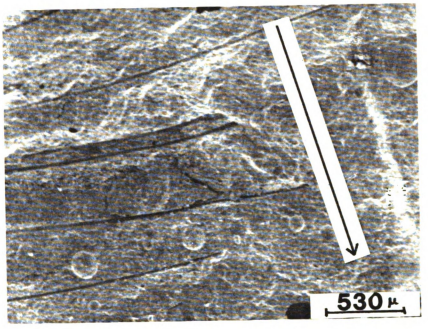


FIGURE 5: Micrographs of the discontinuously reinforced composites illustrating a large fraction of the reinforcements oriented with their long transverse faces perpendicular to the direction of compaction

TABLE 3: Experimentally measured composite fracture toughness in two different directions. These directions are identified in Figure 2.

Volume fraction of ribbons 5.8%

Dimensions of the ribbons length 0.5 cm

width 0.5 cm

thickness 25 micrometers

| Direction | Average composite fracture toughness $K_{IC}$ (MPa $m^{1/2}$) | Coeff.of Variation (%) |
|---|---|---|
| L | 2.67 | 8.9 |
| T | 2.16 | 11.5 |

non-uniform ribbon distribution.

In order to characterize such discontinuous metallic-glass ribbon reinforced composites, it is necessary to examine the load transfer mechanism in such systems. Previous studies [8] carried out on such composites have indicated that both the ribbon length and width affect the load transfer in such composites. The two important equations developed as a result of that analysis are

$$\sigma_c^* = \frac{2\tau V_f(w + t)\ell_c}{wt} \exp[-(\ell_c - x)] + (\sigma_m^* V_m)$$

and

$$\sigma_{cm}^* = \sigma_f^* V_f = \frac{2\tau V_f(w + t)\ell_c}{wt}$$

where, $\sigma_c^*$ is the composite fracture strength

$\sigma_{cm}^*$ is the maximum composite strength

$\sigma_f^*$ is the ribbon fracture strength

$\sigma_m^*$ is the matrix fracture strength

$V_f$ is the volume fraction of the ribbons

$V_m$ is the volume fraction of the matrix

x is the ribbon length

$\ell_c$ is the critical ribbon length (for this geometry $\ell_c = 2/w$)

w is the ribbon width, and

t is the ribbon thickness.

These equations were developed assuming perfect bonding between the matrix and the reinforcements, and assuming load transfer from the matrix to the ribbons occurred by shear. The exponential term in Equation 1 was obtained by experimental data fitting and satisfying the boundary conditions; for x = 0 (no ribbon), $\sigma_c^* = \sigma_m^* V_m$, and for $x = \ell_c$, $\sigma_c^* = \sigma_{cm}^*$.

According to Equation 1, increasing the ribbon length (till $\ell_c$) causes an increase in the strength of the composite. The maximum composite strength is obtained for a ribbon length of $\ell_c$ (Equation 2). The critical ribbon length depends on the width of the ribbon. Increasing the ribbon width decreases the critical ribbon length required for maximum load transfer.

A comparison between the theoretically predicted strength and experimental results can be seen in Figure

6. A, B, C, D, E and F represent curves for different volume fractions and critical lengths of reinforcements. These curves were plotted by using Equation 1. From this equation it can be seen that the maximum load transfer for a given ribbon width is obtained for the same critical ribbon length. However, the maximum load carried depends on the volume fraction of the reinforcements (and increases with increasing volume fraction of reinforcements). A, C, D and E represent curves plotted by using the critical length corresponding to a ribbon width of 0.5 cm, and different volume fractions of ribbon reinforcements. B and F represent curves corresponding to a ribbon width of 0.25 cm (but with different volume fractions of ribbon reinforcemnets). It can be seen that the ribbon width affects the critical ribbon length (compare curves A with B and curves E with F) but not the maximum load carried. The experimental results obtained are in agreement with the theoretically proposed model [8].

The studies have indicated the feasibility of developing discontinuous metallic-glass ribbon reinforced glass-ceramic matrix composites with structural capabilities. Although some information on the load transfer in such composites has been obtained,

FIGURE 6: Plot of the composite strength as a function of the ratio of ribbon length to width.
Solid curves A,B,C,D,E and F are obtained by using equations 1 and 2.
($V_f$ is the volume percent of the ribbon reinforcements and w is the ribbon width.)

A : $V_f$ = 5.8% and w = 0.5 cm

B : $V_f$ = 5.8% and w = 0.25 cm

C : $V_f$ = 3.5% and w = 0.5 cm

D : $V_f$ = 2.5% and w = 0.5 cm

E : $V_f$ = 2.0% and w = 0.5 cm

F : $V_f$ = 2.0% and w = 0.25 cm

The experimentally measured strength values are indicated by various legends as;

(●) $V_f$ = 5.8% and w = 0.5 cm

(▼) $V_f$ = 5.8% and w = 0.25 cm

(▲) $V_f$ = 3.5% and w = 0.5 cm

(■) $V_f$ = 2.5% and w = 0.5 cm

(◆) $V_f$ = 2.0% and w = 0.5 cm

(✱) $V_f$ = 2.0% and w = 0.25 cm

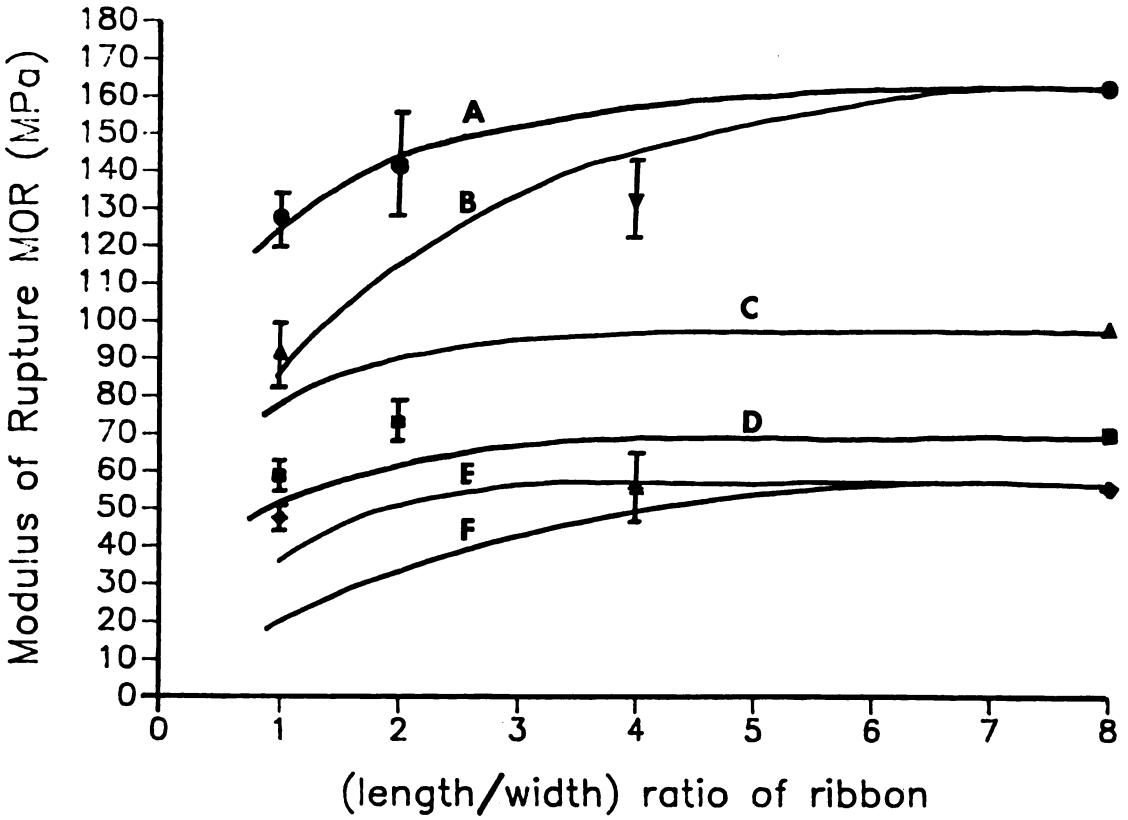
Modulus of Rupture MOR (MPa)
180
170
160
150
140
130
120
110
100
90
80
70
60
50
40
30
20
10
0
0
1
2
3
4
5
6
7
8
(length/width) ratio of ribbon
A
B
C
D
E
F

further studies are necessary to understand the mechanism completely. It is also necessary to test scaled up components in order to investigate the 'size effect' before such composites can be incorporated into structural applications.

## CONCLUSIONS:

From the studies carried out so far it is evident that discontinuous metallic-glass ribbon reinforcements provide an unique method of obtaining isotropic properties in brittle matrix composites. These characteristics are as result of a combination of factors which are 1) the high strength of the ribbons 2) the high interfacial bond strength, and 3) the unique ribbon geometry. The stress transfer in such composites is complex, and depends on both the ribbon length and width. Specifying both these quantities is essential, as they both affect the maximum load carrying capabilities of the system.

**ACKNOWLEDGEMENTS:**

**The authors would like to thank the Composite Materials and Structures Center at Michigan State University for supporting and funding this project.**

**REFERENCES:**


1. Vaidya R. U. and Subramanian K. N., J. Mater. Sci., 25 (1990) 3291.
2. Vaidya R. U. and Subramanian K. N., J. Mater. Sci., (in press).
3. Vaidya R. U. and Subramanian K. N., ASM/ACCE/ESD Conference Proceedings, Detroit Oct. 89., published by ASM, Metals Park OH., pp 227.
4. Vaidya R. U. and Subramanian K. N., J. Am. Ceram. Soc., (in press).
5. Vaidya R. U., Lee T. K. and Subramanian K. N., Fifth annual American Society for Composites (ASC) Coference Proceedings, East Lansing, June 90., published by Technomic press, Lancaster PA., pp 902.
6. Strife J. R. and Prewo K. M., J. Mater. Sci., 17 (1982) 359.
7. Strife J. R. and Prewo K. M., AFWAL Report TR-80-4060 1980.
8. Vaidya R. U. and Subramanian K. N., manuscript submitted to Comp. Sci. and Tech.

# APPENDIX

**ABSTRACT:**

The role of metallic-glass ribbons in modifying the properties of glass-ceramics was investigated by using specimens prepared by conventional pressing and sintering techniques. Even very low volume fractions of such reinforcements were found to provide significant improvements in the strength, elastic properties and fracture toughness of the glass-ceramic matrices. The observed improvement in the fracture toughness is explained on the basis of various metallic-glass ribbon related energy absorbing mechanisms.

## INTRODUCTION:

Enhancement in the tensile strength and fracture toughness of ceramics has been attempted by several techniques such as microcrack toughening and transformation toughening [1-4]. Recent studies have shown that reinforcing ceramics with high strength reinforcements is a viable alternative. In these studies glass, conventional crystalline ceramics or glass-ceramics are used as the matrices[5-7]. Potentials of various reinforcements including continuous and discontinuous fibers(or whiskers) of carbon, graphite, silicon carbide, alumina and various metals like stainless steel and tungsten have been investigated [5-11].

Among the various ceramic matrices, glass-ceramics possess unique advantages. They are formed in the glassy state and are converted to an almost 100% crystalline state by subsequent heat treatment. Such a feature facilitates low temperature composite fabrication and at the same time provides for a composite with high temperature capabilities (without softening). Conventional crystalline ceramics(which are formed by sintering powders) possess significant

porosity, which limits their strength. Glass-ceramics on the other hand have little or no porosity, and hence are tougher and stronger.

Potential of metallic glass ribbons as reinforcements for ceramic matrix composites has not been explored so far. Metallic glasses possess superior fracture strengths and toughness as compared to their crystalline counterparts. Metallic glasses also possess good oxidation and corrosion resistance. Their unique geometry provides for a large surface area to bond with the matrix. Metallic glasses have been studied as reinforcements for brittle polymer matrices by Hornbogen et al [12-14]. Significant improvement in the mechanical properties of the polymer matrices were reported by them. The main objective of the present study was to develop metallic ribbon reinforced glass-ceramic matrix composites and to evaluate their mechanical properties. The nature of the metallic glass/glass-ceramic interface and its role on the mechanical properties of the composite system was also of interest.

## EXPERIMENTAL PROCEDURE:

### Specimen preparation:

Two metallic glasses were used as reinforcements in the present study; one was an iron-based metallic glass METGLAS 2605S-2 alloy, and the other a nickel-based metallic glass METGLAS MBF-75 alloy. Both of these metallic glasses were obtained from Metglas Products, a buisness unit of Allied-Signal Inc. The composition and properties of these metallic glasses as provided by the manufacturer are listed in Table 1.

Based on initial experimentation and on the basis of the low recrysatllization temperatures of the two chosen metallic glasses, Corning glasses Code 7572 and 8463 were chosen as matrices. The compositions and properties of both these glasses as provided by the manufacturer are listed in Table 2.

Rectangular bar shaped specimens(6.25cm x 1.25cm x0.5cm) were made using the conventional wet pressing and sintering techniques. Amyl acetate(3% of the weight of the glass powders) was used as the binder. After laying out the metallic glass ribbons unidirectionally within the glass powders in a steel

TABLE 1: Properties of the metallic glass ribbons.

| Property | METGLAS 2605S-2† | METGLAS MBF-75† |
|---|---|---|
| Chemical composition : | Fe : 78%<br>B : 13%<br>Si : 9% | Ni : 50%<br>Co : 23%<br>Cr : 10%<br>Mo : 7%<br>Fe : 5%<br>B : 5% |
| Crystallization temp. : | 550°C | 605°C |
| Elastic modulus : | 85 GPa | 70 GPa |
| Yield strength : | > 700 MPa | 1300 MPa |
| Coefficient of thermal expansion : | $76 \times 10^{-7}$/ °C | $78 \times 10^{-7}$/ °C |
| Density : | 7.18 g/cc | 7.46 g/cc* |

† Code numbers of products of Metglas Products.
* Obtained from Ref. [22]. Rest of the entries provided by the manufacturer.

TABLE 2: Properties of the ceramic glass matrices (as specified by the manufacturer).

| Property | Corning Glass 7572[@] | Corning Glass 8463[@] |
|---|---|---|
| Softening point : | 375°C | 370°C |
| Coefficient of thermal expansion : | 95 x $10^{-7}$/ °C | 105 x $10^{-7}$/ °C |
| Density (powder) : | 3.8 g/cc | 3.8 g/cc |
| (fired) : | 6.0 g/cc | 6.2 g/cc |
| Continuous service temperature : | 450°C | 450°C |
| Chemical composition : | PbO : 70% | PbO : 84% |
| | $B_2O_3$ : 5-10% | $B_2O_3$ : 5-10% |
| | $SiO_2$ : 2-5% | $SiO_2$ : 2-5% |
| | $Al_2O_3$ : 1-5% | $Al_2O_3$ : 1-5% |
| | ZnO : 10-20% | ZnO : 10-20% |

[@] code numbers of products of Corning Glass Co.

die, the composite specimens were pressed at 3000 psi. After pressing, the specimens were first kept at 200$^{o}$C for 15 minutes to drive out the organic binder. The specimens were then sintered at 400$^{o}$C for 90 minutes. Devitrification of the glassy matrix was carried out by maintaining the composites at 450$^{o}$C for 20 minutes. After this treatment the specimens were furnace cooled to room temperature so as to minimize the thermal shock.

Testing procedures:

The elastic properties of the unreinforced matrix specimens and composite specimens were obtained by the non-destructive Sonic Resonance Technique [15]. Since it was difficult to detect the torsional resonance frequency, the shear modulus was determined by using the values of the Young's modulus (which was obtained from the flexural resonant frequency), and by assuming a Poisson's ratio of 0.25 for the composite system.

Modulus of Rupture (MOR)measurements were made by using the three point bend test in an Instron testing machine with a cross head speed of 0.05cm/min. The span to depth ratio for the specimens was

maintained in accordance with ASTM specification C-203/85.

Static fracture toughness tests were performed by fracturing Single Edge Notched Beam (SENB) specimens, in three point bending. The notches were cut using a diamond blade. The specimens were annealed after cutting the notch, at 200$^{o}$C, to heal up microcracks which might have formed at the root of the notch. The fracture toughness was determined using the equations given by Gross and Srawley [16]. The fracture toughness values for the unreinforced matrix specimens were also determined by the non-destructive indentation technique [17-18]. The specimen were indented using a Vicker's indenter with a load of 0.3 kg. The fracture toughness was determined by using the equations given by Lawn et al [17].

The pull-out test was carried out in order to evaluate the interfacial bond strength. An embedded length of 1.0 cm of ribbon(and width of 0.5cm) was used for this purpose. In such a technique the interfacial bond strength can be determined by balancing the tensile forces to the shear forces acting on the embedded portion of the ribbon.

Fractographic studies were carried out using a Scanning Electron Microscope.

## RESULTS AND DISCUSSION:

### Elastic properties:

The values of the elastic properties of the unreinforced matrix and composite specimens as measured by the Sonic Resonance Technique, are presented in Table 3. A significant improvement in the elastic properties is observed, even with the low volume fraction of reinforcements used. The "Rule of mixtures"(ROM) as used to characterize the elastic properties of several composite systems is given by the equation

$$E_c = E_m V_m + E_f V_f$$

where, `E' denotes the Young's modulus,`V' the volume fraction and the subscripts`c',`m' and`f' refer to the composite, matrix and ribbon respectively. The calculated values of`E' by using the ROM are compared with the experimentally measured values, in Table 4. As is evident from the results, the ROM does not

TABLE 3: Elastic properties of the glass-ceramic matrices and composite systems obtained by the Sonic Resonance Technique.

| Glass-Ceramic Matrix ( Corning Code ) | Metallic-glass Reinforcement (METGLAS alloy) | Volume Fraction of reinforcement | E (GPa) | % increase in E |
|---|---|---|---|---|
| 7572 | - | 0% | 33.4 | - |
| 7572 | 2605S-2 | 0.73% | 44.0 | 31.7 |
| 7572 | 2605S-2 | 1.24% | 47.7 | 42.8 |
| 7572 | 2605S-2 | 1.64% | 69.4 | 108.0 |
| 7572 | MBF-75 | 0.74% | 42.1 | 25.9 |
| 8463 | - | 0% | 28.1 | - |
| 8463 | MBF-75 | 0.69% | 36.0 | 28.0 |
| 8463 | MBF-75 | 0.73% | 40.8 | 45.4 |

TABLE 4: Comparison of the experimentally measured and calculated(by ROM) values of Young's modulus for the METGLAS 2605S-2 alloy reinforced 7572 glass-ceramic system.

| Volume fraction of reinforcement (%) | Young's modulus calculated by ROM (GPa) | Young's modulus measured experimentally (GPa) |
|---|---|---|
| 0.73 | 33.78 | 44.03 |
| 1.24 | 34.04 | 47.70 |
| 1.64 | 34.24 | 69.43 |

characterize the elastic modulus of the composite system under consideration. A better estimate of `E' can be made by considering the equation given by Halpin and Tsai [19-20], according to which

$$\frac{E_c}{E_m} = \frac{1 + \eta \xi V_f}{1 - \eta V_f}$$

where, is the reinforcing efficiency, which will be equal to one for a strongly bonded system, and is an empirical constant which depends on parameters like reinforcement aspect ratio, and bond strength.

The value of ` $\xi$ ' can be obtained by fitting the experimentally obtained values of `E' to the equation given by Halpin and Tsai. For the system under consideration the value of ` $\xi$ ' is evaluated to be 0.24 (Figure 1). The value of the reinforcing efficiency ` $\eta$ ' was assumed to be unity since strong bonding was observed between the ribbon and the matrix (Figure 2).

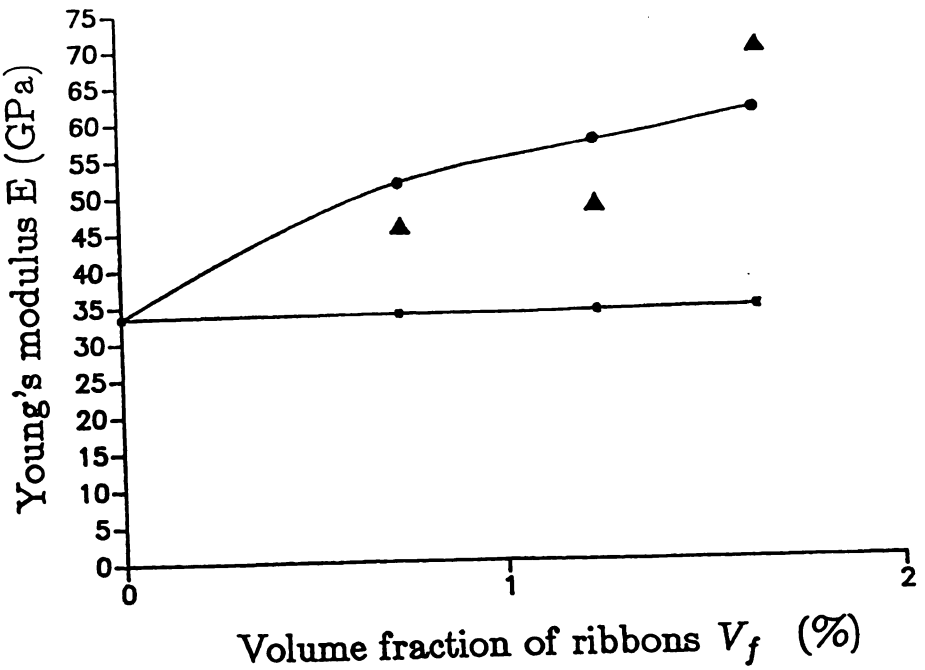


FIGURE 1: Plot of the Young's modulus of the METGLAS 2605S-2 alloy reinforced 7572 matrix composites as a function of volume fraction of metallic glass reinforcement.

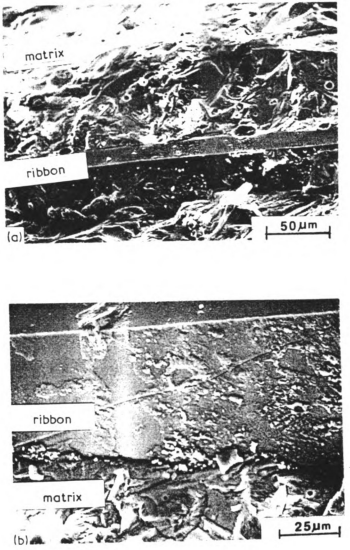


FIGURE 2: Strong(void free) bonding between the METGLAS 2605S-2 alloy ribbon and 7572 matrix.

(a) The matrix is observed to be almost 100% crystalline.

(b) Matrix material adhering to the ribbon surface.

**Strength:**

The Modulus of Rupture (MOR) values of the unreinforced matrix and the composite specimens are presented in Table 5. In the system under consideration, the reinforcing ribbons not only have a higher fracture stress but also a higher fracture strain as compared to the matrix. In the initial stages of loading (in three point bending), the matrix carries a major portion of the load. When the fracture strength of the matrix is reached, the matrix cracks and the load is transferred to the reinforcing ribbons. Two different failure sequences can be enviasged depending upon the volume fraction of reinforcements used. For low volume fractions, when the matrix cracks, the transfer of the load to the ribbons overloads them and they fail. Hence,

$$\sigma_c^* = \sigma_m^* V_m + \sigma_f' V_f$$

where, $\sigma_c^*$ is the fracture stress of the composite
$\sigma_m^*$ is the fracture stress of the matrix, and
$\sigma_f'$ is the stress transferred to the ribbons when the matrix cracks

TABLE 5: Results of the three point bend tests carried out on the glass-ceramic matrices and composite specimens.

| Glass ceramic Matrix ( Corning Code ) | Metallic-glass Reinforcement (METGLAS alloy) | Volume fraction of reinforcement | MOR (MPa) | % increase in MOR | E (GPa) |
|---|---|---|---|---|---|
| 7572 | - | 0% | 14.98 | - | 26.15 |
| 7572 | 2605S-2 | 0.80% | 28.25 | 88.59 | 5.32* |
| 7572 | 2605S-2 | 1.24% | 30.22 | 101.70 | - |
| 7572 | 2605S-2 | 1.64% | 41.25 | 175.40 | - |
| 7572 | MBF-75 | 0.74% | 32.27 | 115.39 | - |
| 7572 | MBF-75 | 1.01% | 33.25 | 121.96 | - |
| 8463 | - | 0% | 11.30 | - | - |
| 8463 | MBF-75 | 0.68% | 20.42 | 80.70 | - |
| 8463 | MBF-75 | 0.69% | 21.62 | 91.33 | - |
| 8463 | MBF-75 | 0.71% | 22.60 | 100.00 | - |
| 8463 | MBF-75 | 0.73% | 23.16 | 104.95 | - |
| 8463 | MBF-75 | 0.77% | 25.3 | 124.20 | - |

* value which does not agree with that obtained by the Sonic Resonance Technique.

When the volume fraction of the reinforcements is high, the transfer of load to the ribbons is not sufficient to fracture them and they continue to carry the load until their fracture strength is reached. Under these conditions

$$\sigma_c^* = \sigma_f^* V_f$$

where, $\sigma_f^*$ is the fracture stress of the ribbons.

The cross over point between these two behaviours occurs at a critical volume fraction $V_c'$, where

$$V_c' = \frac{\sigma_m^*}{\sigma_m^* + \sigma_f^* - \sigma_f'}$$

For the composite system under consideration the calculated value of $V_c'$ is 0.5%. All the composite specimens used in the current study had a volume fraction of reinforcements greater than this critical volume fraction. Hence the strength of the composite

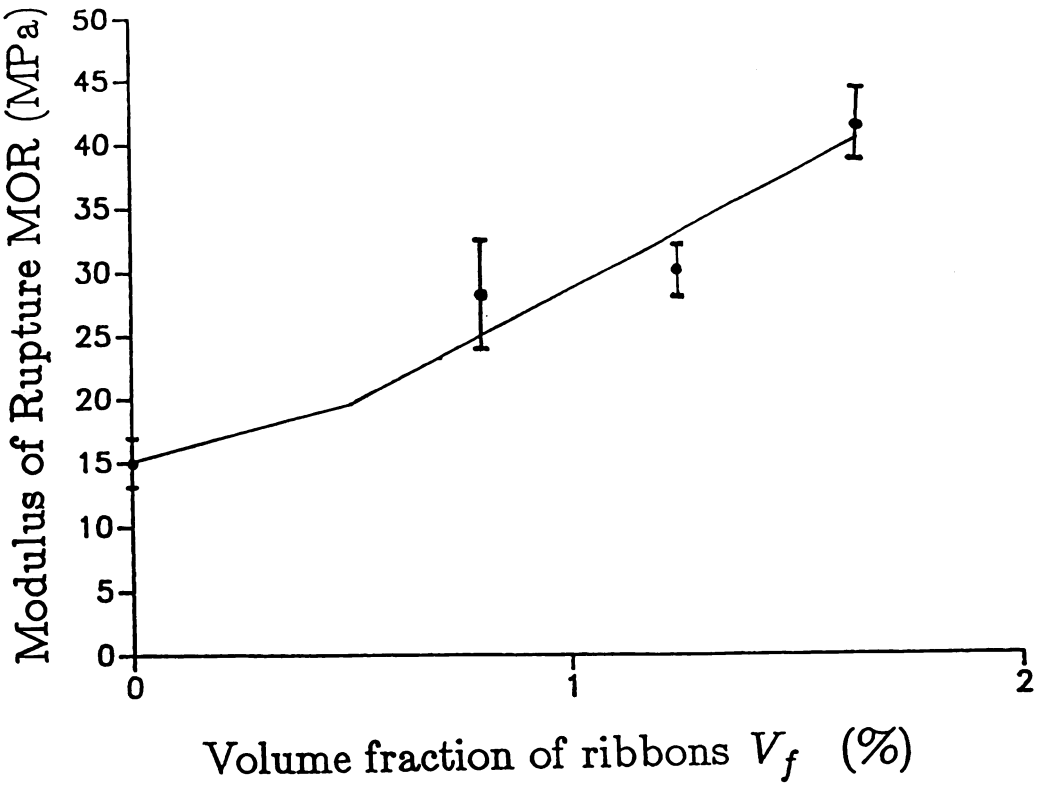


FIGURE 3: Plot of the fracture strength of the METGLAS 2605S-2 alloy reinforced 7572 matrix composites as a function of volume fraction of metallic glass reinforcement.

specimens is essentially a function of the volume fraction of the metallic glass reinforcements. Higher volume fractions of reinforcements should show significant improvements in the fracture strength. The variation in the MOR of the composite specimens with increasing volume fraction of metallic glass reinforcements is illustrated in Figure 3.

The Young's modulus (E) of the specimens was also calculated from the results of the three point bend test. The values of `E' obtained from the three point bend test with those obtained from the Sonic resonance test are compared in Table 6. The values of `E' obtained for the unreinforced matrix specimen by both the techniques agree well; on the other hand the values obtained for the composite specimen do not. This discrepency may be attributed to the non-uniform load carring characteristics of the composite system.

Fracture toughness:

The fracture toughness values for the unreinforced matrix and composite specimens as measured by the Single Edge Notched Beam technique, are listed in Table 7. The fracture toughness values for the unreinforced matrix specimens as measured by the

TABLE 6: Comparison of the values of the Young's modulus of the METGLAS 2605S-2 alloy reinforced 7572 glass-ceramic specimens obtained from the Sonic Resonance and Three Point Bend tests.

| Test | Average Young's Modulus 7572 matrix (GPa) | Average Young's Modulus 7572 + 2605S-2 composite (GPa) |
|---|---|---|
| Dynamic Resonance | 33.40 | 44.00 |
| Three point bending | 26.15 | 5.32 |

TABLE 7: Fracture toughness obtained by the Notched Beam tests.

| Sample | $K_{IC}$ ($MPam^{1/2}$) | Average $K_{IC}$ ($MPam^{1/2}$) | Standard Dev ($MPam^{1/2}$) | Coeff.of Variation |
|---|---|---|---|---|
| 7572 matrix | 0.4046<br>0.3580<br>0.3730 | 0.378 | 0.0237 | 6.26% |
| 7572 matrix reinforced with 0.6% METGLAS 2605S-2 | 1.0886<br>0.8320<br>1.1800<br>0.7080 | 0.952 | 0.3022 | 31.74% |
| 7572 matrix reinforced with 1.24% METGLAS 2605S-2 | 1.372<br>1.430 | 1.401 | 0.041 | 2.93% |

Indentation technique, are listed in Table 8. The indentation technique cannot be used to measure the fracture toughness of the composite specimens because the reinforcing ribbons are positioned far away from the surface(where the indentation is carried out), and as a result do not affect the crack growth behaviour at the indentatation. A plot of the fracture toughness versus the volume fraction of metallic glass reinforcements is provided in Figure 4. A clear enhancement in the fracture toughness with respect to the unreinforced matrix is evident from this plot. This behaviour can be attributed to improvements in the various mechanical properties such as Young's modulus, fracture stress and fracture strain, which can be correlated to the fracture toughness using the empirical equation given by Hahn and Rosenfield [21], according to which

$$K_{Ic} = (E \quad \sigma_f \quad \epsilon_f L)^{0.5}$$

where, $K_{Ic}$ is the fracture toughness

$\sigma_f$ is the fracture stress

$\epsilon_f$ is the fracture strain, and

L is a geometrical correction factor.

In the system studied, the Young's modulus,

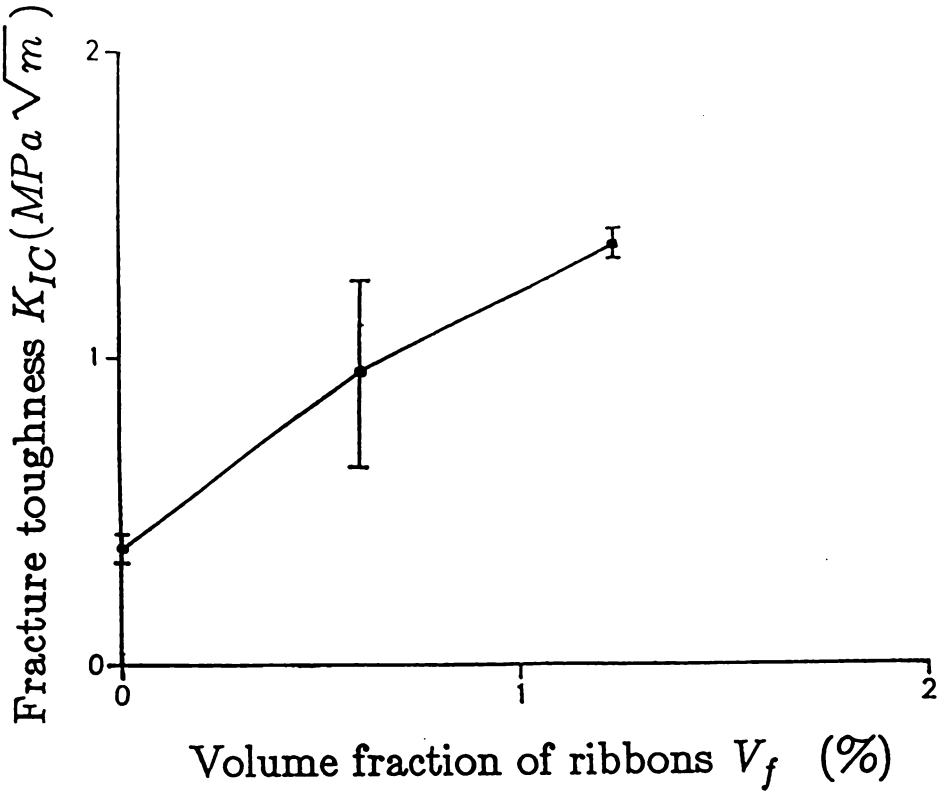


FIGURE 4: Plot of the fracture toughness of the METGLAS 2605S-2 alloy reinforced 7572 matrix composites as a function of volume fraction of metallic glass reinforcement.

TABLE 8: Fracture toughness obtained by the Indentation technique.

| | | |
|---|---|---|
| Specimen : | Lead Borosilicate glass, code 7572. | |
| Indentation load : | 0.3 Kg. | |
| Loading time : | 20 seconds. | |
| Loading speed : | 50 micometers/sec. | |
| Number of specimens : | 3 | |
| Indentations per specimen : | 25 | |
| Fracture toughness : $K_{IC}(MPam^{1/2})$ | 0.496<br>0.433<br>0.450 | Average : 0.46 |
| Standard deviation : | 0.0327 $MPam^{1/2}$ | |
| Coeff.of Variation : | 7.11% | |

fracture stress and fracture strain all increase with increasing volume fraction of reinforcements, and hence the fracture toughness is also expected to improve. The improvement in the fracture toughness can also be explained on the basis of fracture energy considerations. The fracture toughness is related to the Young's modulus and fracture energy ($G_{Ic}$) by the equation

$$K_{Ic} = (E\ G_{Ic})^{0.5}.$$

The total energy absorbed during fracture of the composite is the sum of the energies absorbed by the matrix related processes ($G_m$) and by the ribbon related processes ($G_f$).
Hence,

$$G_{Ic} = G_f V_f + G_m V_m.$$

The contribution to $G_f$ arises from four different ribbon related processes. In addition to energy absorbed by ribbon failure (specific ribbon fracture energy $w_f$), energy is also dissipated as a result of ribbon-matrix debonding ($w_d$)and ribbon pullout ($w_p$). Furthermore there exists a bending component ($w_b$)as the crack in the surrounding matrix opens before the reinforcing component is broken.

Hence,

$$G_f = w_p + w_b + w_d + w_f$$

It is believed that this crack deflection at the ribbon-matrix interface, strengthens the composite and makes it tougher by causing secondary processes such as debonding and pullout to come into play, thereby absorbing energy. This particular phenomenon can be observed in Figure 5. Another mechanism of energy absorption is the initiation of secondary cracks at the edges of the reinforcing ribbons(Figure 6). These are created when under the influence of bending moments, the sharp edges of the ribbons tend to wedge open the brittle matrix. The ribbons can also be assumed to exhibit higher fracture strengths as a result of hinderance of shear failure due to the surrounding rigid matrix, increasing the contribution to $w_f$ (Figure 7).

A very strong bond between the ribbon and matrix was observed, as was evidenced by the absence of ribbon-matrix debonding in the pull out test. Hence the $w_d$ and $w_p$ contributions are low in case of the system under consideration. The main contribution to the fracture energy of the present system are believed

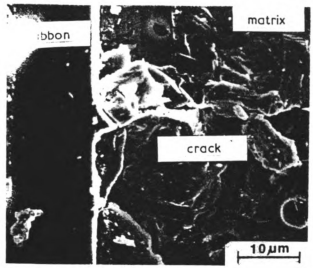


FIGURE 5: Crack arrest and deflection at the metallic glass ribbon (METGLAS 2605S-2)-matrix (7572)

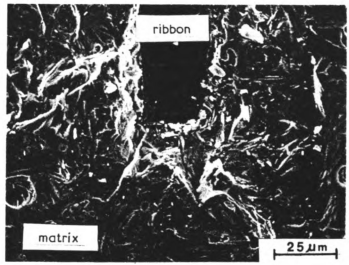


FIGURE 6: Microcracks originating at the edges of the reinforcing ribbons (METGLAS 2605S-2) in the 7572 matrix.

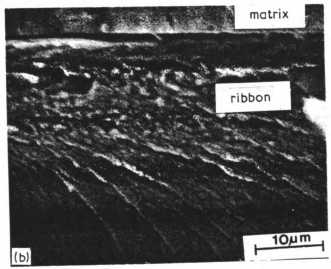


FIGURE 7: Micrographs illustrating the high ductility of the metallic glass ribbons.

(a) A crushed ribbon (METGLAS 2605S-2) in composite failure.

(b) Vein type of fracture pattern on the metallic glass (METGLAS 2605S-2) ribbon surface. interface. The crack originated at the tensile surface during the bend test.

to arise from the $w_f$ and $w_b$ components.

**CONCLUSIONS:**

1. Introduction of even a very low volume fraction of metallic glass reinforcements, provide significant improvements in the elastic properties, fracture strength and fracture toughness of the brittle glass-ceramic matrices. The strength of the composite system is a function of the fracture strength and the volume fraction of the ribbons, and increases proportionately with increasing volume fraction of reinforcements.

2. The elastic properties of the present composite system do not obey the rule of mixtures. They can be predicted by using the empirical equation given by Halpin and Tsai [19-20].

3. The improvement in the fracture toughness of the present composite system is due to the introduction of various ribbon related energy absorbing mechanisms such as crack arrest and deflection and elastic bending and fracture of the ribbons. Microcracking of the matrix at the edges of the ribbons also contributes to the fracture toughness.

**ACKNOWLEDGEMENTS:**

The authors would like to acknowledge the Composite Materials and Structures Center at Michigan State University for supporting and funding this project. The authors would also like to extend their sincere thanks to Dr. Kenneth Chyung of Corning Glass Works for providing the glass powders, and to Dr. Edward Norin of Metglas Products for providing valuable suggestions in the preparation of this manuscript.

**REFERENCES:**


1. K. Faber and A. Evans, J. Am. Ceram. Soc., 67 (1984) 255.
2. A. Evans and A. Heuer, J. Am. Ceram. Soc.,63 (1980) 241.
3. A. Evans, "Advances in ceramics" Volume 12, Edited by N. Claussen, M. Ruhle and A. Heuer, publishers Am. Ceram. Soc., Ohio 1984, p 193.
4. R. McMeeking and A. Evans, J. Am. Ceram. Soc.,65 (1982) 242.
5. R. Sambell, D. Brown and D. Phillips, J. Mat. Sci., 7 (1972) 663.
6. R. Sambell, D. Brown and D. Phillips, ibid 7 (1972) 676.
7. M. Sahebkar, J. Schlichting and P. Schubert, Berichte de Deutschen Keramischen Gesellschaft, 55 (1978) 265.
8. K. Gadkaree and K. Chyung, Am. Ceram. Soc. Bull.,65 (1986) 370.
9. P. Shalek, J. Petrovik and F. Gac, Am. Ceram. Soc. Bull., 65 (1986) 351.
10. S. Risbud and M. Herron, Am. Ceram. Soc. Bull., 65 (1986) 342.
11. A. Caputo, D. Stinton and T. Besmann, Am. Ceram.

Soc. Bull., 66 (1987) 368.

12. A. Fels, K. Friedrich and E. Hornbogen, J. Mat. Sci. Letters, 3 (1984) 569.

13. A. Fels, K. Friedrich and E. Hornbogen, J. Mat. Sci. Letters, 3 (1984) 639.

14. T. Tio, K. Friedrich, E. Hornbogen, U. Koster and A. Fels, J. Mat. Sci. Letters, 3 (1984) 415.

15. S. Screiber, D. Anderson and N. Soga, "Elastic constants and their measurements", publishers McGraw Hill, New York, 1974, p.82.

16. M. Srinivasan and S. Seshadri, "Fracture mechanics for ceramics, rocks and concrete", ASTM special technical publication Nos. 745, 1977, p.46.

17. B. Lawn, "Fracture mechanics of ceramics" , Vol.5 Edited by R. Bradt, A. Evans and D. P. H. Hasselmann, publishers Plenum press, New York, 1983, p.1.

18. D. Shetty, A. Rosenfield and W. Duckworth, J. Am. Ceram. Soc., 68 (1985) 65.

19 J. Halpin and S. Tsai, Air Force Materials Laboratory Technical Report AFML-TR-67-423, 1967.

20. D. Hull, "An introduction to composite materials", Edited by R. Cahn, E. Davis and I. Ward, publishers Cambridge University Press, Cambridge, 1985, p.127.

21. G. Hahn and A. Rosenfield, Proc. 3rd Int. Conf. on Fracture, Munich, West Germany, 1 (1973) p.13.

22. J. C. M. Li, **"Treatise on Material Science and Technology-Vol 20."**, Edited by Herbert Herman, publishers Academic Press, New York, 1981, p.325.